On modulational instability of nonlinear waves in 1D ferromagnetic spin chains

2005 J. Phys.: Condens. Matter 17 3083

(http://iopscience.iop.org/0953-8984/17/19/021)

INSTITUTE OF PHYSICS PUBLISHING JOURNAL OF PHYSICS: CONDENSED MATTER

J. Phys.: Condens. Matter **17** (2005) 3083–3112 doi:10.1088/0953-8984/17/19/021

On modulational instability of nonlinear waves in 1D ferromagnetic spin chains

Jean-Pierre Nguenang[1,2,3], Michel Peyrard[1], Aurelien J Kenfack[3] and Timoleon C Kofané[3]

[1] Laboratoire de Physique, Ecole Normale Supérieure de Lyon, 46, Allée d'Italie, 69364 LYON Cedex 07, France
[2] Condensed Matter Laboratory, Department of Physics, Faculty of Science, University Of Douala, PO Box 24157, Douala, Cameroon
[3] Laboratoire de Mécanique, Faculté des Sciences, Université de Yaoundé I, BP: 812, Yaoundé, Cameroon

E-mail: nguenang@yahoo.com

Received 7 September 2004, in final form 17 March 2005
Published 29 April 2005
Online at stacks.iop.org/JPhysCM/17/3083

Abstract

We report a theoretical study of modulational instability of extended nonlinear spin waves in a one-dimensional ferromagnetic chain. The investigation is made both analytically within the framework of the linear stability analysis and also numerically by means of molecular dynamics simulations. Using a Holstein–Primakoff transformation for the spin operators, the Hamiltonian, which is constituted by a Heisenberg exchange term, a biquadratic exchange energy, an anisotropic energy and a Zeeman term, is bosonized. Then we derive a discrete nonlinear Schrödinger-like equation for the spin-wave motion. Using a linear stability analysis, we establish the stability criteria of the spin waves in such a ferromagnetic chain. From our numerical simulations of the discrete spin chain for the onset of instability, it emerges that the analytical predictions are correctly verified. For a long timescale, depending on the strength of the biquadratic exchange interaction relative to the exchange energy and the anisotropy energy, on the one hand an intrinsic localized wave train can be created displaying properties of the breather motion. On the other hand, due to the increasing size of the instability domain, with increase of the biquadratic parameter, the instability can fully develop and the linear stability fails; consequently, the time evolution of the modulated spin waves can show both regular and chaotic behaviour.

1. Introduction

Nonlinear excitations in one-dimensional (1D) magnets have generated during the past three decades a great deal of experimental [1–4], and theoretical interest [5–11]. Within the set

of nonlinear excitations in magnetic systems, the most studied is that of soliton type. The soliton solutions for spin chains have been investigated by several different approaches. In the classical approach, general single-soliton solutions are obtained for a continuum version of the classical linear Heisenberg chain [7]. In a quantum spin system, a bosonic representation of spin operators turns out to be a very suitable method for studying the solitary waves, because they allow us to include quantum corrections in a systematic way. In spin coherent representation [12], one can work directly with the operators, make no approximation to the Hamiltonian, and develop an exact nonlinear equation for the quantum system [13], but this method seems to be limited because it works with a limited number of interaction terms in the Hamiltonian. To avoid this limitation, it is necessary to use a truncated Holstein–Primakoff expansion for the spin operators [8, 14]. Then the Hamiltonian can be bosonized. Further, working in the coherent-state representation of Glauber [15], and making small-amplitude and long-wave approximations, one finds solitary-wave profiles identical to classical solitons, which is the so-called semiclassical treatment.

The realization that lattice discreteness can stabilize highly localized excitations in perfect nonlinear and non-integrable lattices has been a very recent conceptual breakthrough in nonlinear dynamics [16, 17]. The analogy between lattice vibrations and spin waves has led to studies of intrinsic localized spin-wave modes (ILSMs) in semiclassical and classical magnetic models [18–32]. The ILSMs are non-topological and can exist in discrete lattices of any space dimension, so they should be contrasted with the continuum topological kink solitons that have been well studied in a 1D magnetic system [7].

In most of the aforementioned studies related to ILSMs of magnetic chains, great efforts have been made in the theoretical details for understanding the important effects of lattices discreteness on intrinsic localization, their existence, their stability and creation criteria in various antiferromagnetic crystals [33]. Meanwhile studies on the ILSMs were done in antiferromagnets; research was also growing on the stability of the extended nonlinear excitations in antiferromagnetic systems [33]. However, only very few studies on ILSMs of nonlinear extended spin waves have been devoted to the ferromagnetic systems. For instance, the important problem of the existence and stability of extended nonlinear spin-wave excitations in ferromagnetic systems is still an open question. The modulational instability of extended (MIE) nonlinear spin waves, which is a good method to answer the above-mentioned open question, can be treated quantitatively by different approaches. We use here the method of second quantization based upon the creation and annihilation magnon operators, obtained from the spin operators with the Holstein–Primakoff transformation [8]. From this point of view, the MIE can be understood as a mechanism for dynamical localization of spin waves in homogeneous magnetic lattices. Since the dissipation of spin waves in magnetic materials is weak compared to that in lattice vibration in crystals, from a theoretical and an experimental point of view nonlinear ferromagnetic systems may provide more tractable candidates for the investigation of ILSMs and modulational instability (MI) of excitations which can be extended at nanoscale dimensions, as well as for future exploration of the quantum properties of such excitations.

This paper aims at carrying out a theoretical analysis, with first an analytical calculation of instability criteria that is based on a discrete nonlinear Schrödinger-like equation obtained after going beyond a second-quantization scheme of the Hamiltonian. Second, with numerical simulations of the modulational instability of the nonlinear extended spin waves, we verified analytical results and put out some new features of these new nonlinear excitations in discrete ferromagnetic system.

The material of this paper is organized as follows. In section 2, we describe the model and introduce the Holstein–Primakoff transformations on the spin operators, and next we derive the

discrete nonlinear Schrödinger-like equation of motion. Section 3 is devoted to the analytical studies of the modulational stability/instability of the extended nonlinear spin waves. We then continue in section 4, where we investigate numerically the accuracy of the analytical results. In section 5, we investigate the different wave pattern formation that the nonlinear extended spin waves may display. Section 6 is devoted to the energy distribution in the ferromagnetic chain, and in section 7 we conclude the paper.

2. Model Hamiltonian and formalism

The model we deal with in this section is a discrete chain of spins interacting by short-range nearest-neighbour ferromagnetic exchange interactions. It is also subject to an anisotropic field perpendicular to the chain direction and an applied magnetic field. Hence, the following Hamiltonian describes it:

$$H = -\frac{J}{2}\sum_{i\rho}\vec{S}_i\vec{S}_{i+\rho} - g\mu_{\mathrm{B}}B_{\mathrm{e}}\sum_i S_i^z + A\sum_i (S_i^z)^2 - \alpha\frac{J}{2}\sum_{i\rho}(\vec{S}_i\vec{S}_{i+\rho})^2 \tag{2.1}$$

where the sums run over the lattice sites separated by a distance a_0 along the Z-axis and the index ρ stands for the nearest neighbour of each spin. Here, S_i^δ ($\delta = x, y, z$) is the δ component of the spin vectors on the ith site. The first term in Hamiltonian (2.1) represents the Heisenberg exchange energy where $J > 0$ is the short-range nearest-neighbour exchange coupling constant. The spin may also be placed in an external field (B_{e}) directed along the Z-axis, leading to the second term, representing the Zeeman energy, where the quantities g and μ_{B} are the Landé g factor and the Bohr magneton, respectively.

The third term is the single-ion uniaxial anisotropy energy due to the crystalline field. It constrains the spin to lie in a plane perpendicular to the chain axis. A is the uniaxial crystal-field anisotropy parameter.

The fourth term represents the biquadratic isotropic exchange interaction, which should be considered for a high-spin system, with $S \geqslant 1$ [34]. The parameter α measures the strength of the biquadratic exchange, in the classical approximation. Adler gave a discussion of these biquadratic exchange interactions through an extensive review of experimental results, which establish the importance of this term in a variety of compounds [35]. The necessity of including such a term goes back to Schrödinger and the interpretation in terms of a super-exchange mechanism was given by Anderson [36]. Kapor and Skrinjar gave also another interpretation of the biquadratic exchange interaction in terms of a three-spin exchange interaction [37]. For a ferromagnetic ground state, the parameter α has to satisfy, for $S = 1$, $0 < \alpha < 1$, and for a spin with $S > 1$ the condition is $-2/(S(2S-3)) < \alpha < 2(S+1)/S^2$ [34].

Since we are going to use a semi-classical treatment in our study and in order to bosonize Hamiltonian (2.1), we need to treat this Hamiltonian (2.1) in the Holstein–Primakoff representation for the spin operator

$$\tilde{S}_i^+ = \sqrt{2}(1-\varepsilon^2 a_i^+ a_i)^{1/2}\varepsilon a_i = \sqrt{2}[1-\varepsilon^2 a_i^+ a_i/4 - \varepsilon^4 a_i^+ a_i a_i^+ a_i/32 + \mathrm{O}(\varepsilon^6)]\varepsilon a_i \tag{2.2a}$$

$$\tilde{S}_{i^-} = \sqrt{2}\varepsilon a_i^+(1-\varepsilon^2 a_i^+ a_i)^{1/2} = \sqrt{2}\varepsilon a_i^+[1-\varepsilon^2 a_i^+ a_i/4 - \varepsilon^4 a_i^+ a_i a_i^+ a_i/32 + \mathrm{O}(\varepsilon^6)] \tag{2.2b}$$

and

$$\tilde{S}_i^z = 1 - \varepsilon^2 a_i^+ a_i \tag{2.2c}$$

where $\varepsilon = \frac{1}{\sqrt{S}}$ and $\tilde{S}_i = \frac{S_i}{S_c}$. $S_c = \hbar S$ and the condition $S_c = \lim_{S\to\infty}^{\hbar\to 0}(\hbar S)$ is the semi-classical limit. Next, we introduce the dimensionless variable for the Hamiltonian

$$\tilde{H} = \frac{H}{J(S_c)^2}. \tag{2.2d}$$

By substituting equations (2.2) into (2.1), we get after retaining terms of order $O(\varepsilon^6)$ the Hamiltonian

$$\tilde{H} = G(a_i^+, a_i, a_{i+\rho}^+, a_{i+\rho}) + O(\varepsilon^6) \tag{2.3}$$

where G is the expression of H in terms of the boson creation and annihilation operator a_i^+, a_i, $a_{i+\rho}^+$, $a_{i+\rho}$ forms, in different sites of the spin chain. It is well known that the Bose operators satisfy the following Heisenberg equation of motion:

$$\mathrm{i}\left(\frac{\varepsilon^2}{JS_c}\right)\frac{\partial a_n}{\partial t} = [a_n, \tilde{H}]. \tag{2.4}$$

Then we calculate the commutation function expressed by $[a_n, \tilde{H}]$, and now we find the equation of motion expressed by the bosonic operators a_n^+, a_n, provided that they fulfil the commutation rules, i.e. $[a_m, a_n^+] = \delta_{mn}$, with $\delta_{nm} = 0$ if $n \neq m$, or $\delta_{nm} = 1$ if $n = m$. Then, we obtain an equation in the form

$$\mathrm{i}\frac{\partial a_n}{\partial t} = F(a_n^+, a_{n,} a_{n+\rho}^+, a_{n+\rho}). \tag{2.5}$$

Since we are concerned with extended nonlinear excitations of spin induced by nonlinearity in the magnon system in equation (2.3), in which a cluster of spin may undergo a large excursion as compared with the rest of the spins, a physically acceptable candidate for quantum states of such large-amplitude collective modes may be coherent states [38]. Therefore, we follow our study by employing the coherent-state ansatz for the eigenfunction $\psi_n(t)$ of the Hamiltonian H

$$\psi_n(t) = \Pi_n \exp\left(-\tfrac{1}{2}|\psi_n|^2\right) \times \exp(\psi_n a_n^+)|0\rangle \tag{2.6}$$

that defines the pure coherent state with $|\psi_n(t)\rangle$, that represents the coherent-state eigenvector, which is non-orthogonal and over-complete, and in which $|0\rangle$ defines the vacuum eigenstate of the boson system. This said, for a given state vector $|\varphi_n\rangle$ defined by the relation

$$|\varphi_n\rangle = \Pi_n|\psi_n\rangle \tag{2.7a}$$

the following properties are fulfilled.

$$a_n^+|\varphi_n\rangle = \psi_n^*(t)|\varphi_n\rangle \tag{2.7b}$$

$$a_n|\varphi_n\rangle = \psi_n(t)|\varphi_n\rangle. \tag{2.7c}$$

The expectation value of a Hamiltonian operator in equation (2.3) in the state $|\varphi_n\rangle$ can be obtained using the diagonal matrix elements of $\langle\varphi_n|H(a_n^+, a_n, a_{n+\rho}^+, a_{n+\rho})|\varphi_n\rangle$. These elements are known to be good operator representatives [13]. The result is therefore a real scalar function expressed by a dimensionless Hamiltonian function.

$$\tilde{H} = \tilde{H}(\psi_n^*, \psi_n, \psi_{n+\rho}^*, \psi_{n+\rho}). \tag{2.8a}$$

Thus, using these above-mentioned coherent state properties in the equation of the boson mode motion given in equation (2.5), it emerges that

$$\begin{aligned}\mathrm{i}\frac{\partial \psi_n}{\partial t} = {} & A_1\psi_n + A_2\sum_\rho(\psi_{n+\rho} - \psi_n) + A_3|\psi_n|^2\psi_n \\ & + A_4\sum_\rho(|\psi_n|^2\psi_{n+\rho} + |\psi_{n+\rho}|^2\psi_{n+\rho} + \psi_n^2\psi_{n+\rho}^*). \\ & + A_5\sum_\rho|\psi_{n+\rho}|^2\psi_n - A_6\sum_\rho\psi_{n+\rho}^2\psi_n^*.\end{aligned} \tag{2.8b}$$

Here the index ρ still stands for the nearest neighbours of a spin on the lattice site n. In the next calculations we chose the particular values of $\rho = \pm 1$. Before continuing, it is important

to specify that in the low-temperature excitations the introduction of a coherent state helps in projecting out the unphysical boson states, provided that no essential information is lost in this treatment. In this respect, working with the boson operators instead of the spin operators that act as circularly polarized variables as in other works in antiferromagnetic chains [26–32] should also lead to keeping essential features of our one-dimensional spin chain.

As we developed above, the framework of our present considerations here is the semi-classical spin theory. The nonlinear differential-difference equation (2.8*b*) is a modified discrete nonlinear Schrödinger-like equation. It defines the collective excitations for the boson mode of a discrete spin lattice. It is extremely difficult to perform a complete analysis of equation (2.8*b*) analytically. But a continuum approximation can be used to approach analytical soliton solutions of such a system [8, 34]. Since we are interested in modulational instability of the extended nonlinear excitations that may arise from such a discrete system, we shall then follow by performing an analytical calculation as well as a numerical computation for such a study.

3. Modulational instability of the extended nonlinear spin wave

The modulational instability of a plane wave in such a magnetic spin lattice is investigated by studying the stability of its amplitude in the presence of sufficiently small perturbation so that one can linearize the equation of the envelope and the carrier wave. Before we continue let us recall that Dauxois and Peyrard have shown that the modulational instability of a linear wave is a first step towards energy localization in nonlinear lattices [23]. The same phenomenon has been studied in various contexts: in fluid dynamics [39], where it is usually called the Benjamin–Feir instability, nonlinear optics [40] and plasma physics [41]. The first step to probe some particular features of these excitations in a ferromagnetic chain is to introduce a small perturbation in the amplitude and in the phase, and look for the solution of equation (2.8*b*).

3.1. Analytical results

To study the modulational stability/instability of an extended nonlinear wave in such a system, we investigate the time evolution of a perturbed nonlinear wave of the form

$$\psi_n(t) = [\phi_0 + b_n(t)] \exp \mathrm{i}[\theta_n(t) + \varphi_n(t)] \tag{3.1}$$

where $\theta_n(t) = qn - \omega_0 t$, with ω_0 that obeys the nonlinear dispersion relation

$$\omega_0 = A_1 - 2A_2 + (A_3 + 2A_5)\phi_0^2 + (2A_2 + 6A_4\phi_0^2)\cos(q) - 2A_6\phi_0^2\cos(2q) \tag{3.2}$$

ϕ_0 is a constant amplitude of a plane wave; the lattice spacing parameter a_0 is set to unity for the sake of simplicity. Replacing equations (3.1) in (2.8*b*) and assuming $|b_{n(t)}| \ll \phi_0$ and also that $|\varphi_{n(t)}| \ll \theta_n(t)$, and finally also taking into account equation (3.2), we obtain the following system of linear coupled equations:

$$\begin{aligned}\frac{\partial b_n}{\partial t} = {} & A_2\phi_0(\varphi_{n+1} + \varphi_{n-1} - 2\varphi_n)\cos q + A_2(b_{n+1} - b_{n-1})\sin q + A_3\phi_0^3(\varphi_n - \varphi_n^*) \\ & + A_4\phi_0^3(3\varphi_{n+1} + 3\varphi_{n-1} - 2\varphi_n^* - 2\varphi_{n+1}^* - 2\varphi_{n-1}^*)\cos q \\ & + 3A_4\phi_0^2(b_{n+1} - b_{n-1})\sin q + A_5\phi_0^3(\varphi_{n+1} + \varphi_{n-1} - \varphi_{n+1}^* - \varphi_{n-1}^*) \\ & - 2A_6\phi_0^3(\varphi_{n+1} + \varphi_{n-1} - \varphi_n - \varphi_n^*)\cos 2q \\ & - 2A_6\phi_0^2(b_{n+1} - b_{n-1})\sin 2q \end{aligned} \tag{3.3a}$$

$$\begin{aligned} -\phi_0\frac{\partial \varphi_n}{\partial t} = {} & A_2(b_{n+1} + b_{n-1} - 2b_n)\cos q - A_2\phi_0(\varphi_{n+1} - \varphi_{n-1})\sin q + A_3\phi_0^2(b_n + b_n^*) \\ & - 3A_4\phi_0^3(\varphi_{n+1} - \varphi_{n-1})\sin q + A_4\phi_0^2(3b_{n+1} + 3b_{n-1} \end{aligned}$$

$$
\begin{aligned}
&- 2b_n + 2b^*_{n+1} + 2b^*_{n-1})\cos q \\
&+ A_5\phi_0^2(b_{n+1} + b_{n-1} + b^*_{n+1} + b^*_{n-1}) - 2A_6\phi_0^2(b_{n+1} + b_{n-1} + b_n + b^*_n) \\
&\times \cos 2q + 2A_6\phi_0^3(\varphi_{n+1} - \varphi_{n-1})\sin 2q. \qquad (3.3b)
\end{aligned}
$$

Such a linear system of equations has a general solution of the form

$$
\begin{pmatrix} \varphi_n \\ b_n \end{pmatrix} = \begin{bmatrix} \varphi_1 & \varphi_2 \\ b_1 & b_2 \end{bmatrix} \begin{pmatrix} \exp \mathrm{i}(Qn + \Omega t) \\ \exp -\mathrm{i}(Qn + \Omega^* t) \end{pmatrix} \qquad (3.4)
$$

with $b_1, b_2, \varphi_1, \varphi_2$ that are arbitrary real constants, and Q is the wavenumber of the noise. Ω^* is the complex conjugate of the noise's frequency $\Omega = \Omega_\mathrm{r} + \mathrm{i}\Omega_\mathrm{im}$, the index (r) and (im) stand for the real part and imaginary part of the frequency of the noise, respectively. Introducing solution (3.4) in (3.3), we obtain a set of four complex equations. This system leads to two sets of four real equations by cancelling the real and imaginary parts. Then the cancellation of the imaginary part gives a system with the following form:

$$
\begin{pmatrix} c_1 + \sigma_i & c_2 & c_3 & c_4 \\ a_1 & a_2 - \sigma_i & a_3 & a_4 \\ e_1 & e_2 & e_3 + \sigma_i & e_4 \\ d_1 & d_2 & d_3 & d_4 - \sigma_i \end{pmatrix} \begin{pmatrix} \varphi_1 \\ b_1 \\ \varphi_2 \\ b_2 \end{pmatrix} = \begin{pmatrix} 0 \\ 0 \\ 0 \\ 0 \end{pmatrix} \qquad (3.5)
$$

which only has a non-trivial solution if its determinant vanishes. This gives the condition

$$
\sigma_i^4 + \ell_2\sigma_i^2 + \ell_0 = 0 \qquad (3.6)
$$

with $\sigma_i = \phi_0\Omega_\mathrm{im}$ that determines Ω_im. The different components of the matrix are expressed in the appendix. Equation (3.6) can be factorized, thus it is possible to derive the analytical expression of the imaginary part of the frequency of the noise modulating the nonlinear wave in the following implicit forms:

$$
\Omega_\mathrm{im1} = \pm\sqrt{\alpha_1(q, Q)} \qquad \text{and} \qquad \Omega_\mathrm{im2} = \pm\sqrt{\alpha_2(q, Q)} \qquad (3.7)
$$

where $\Omega^2_\mathrm{im1} \cdot \Omega^2_\mathrm{im2} \cdot \phi_0^4 = \ell_0$ and the explicit forms of $\alpha_1(q, Q)$ and $\alpha_2(q, Q)$ are given in the appendix. They show how the stability and instability regions depend not only on q and Q but also on the model parameters. The part of the above-mentioned set of equations that determines the real part of the frequency yields a system which is diagonal. In the corresponding system, all the diagonal terms are equal so that the cancellation of its determinant reduces to a single equation. Therefore, given a wavevector q of an excited wave modulated by a wave with wavenumber Q, for each of the four possible values of the imaginary part of the frequency given in equation (3.7), the corresponding real part of the frequency of the modulating wave in the system has the same value Ω_r, expressed by

$$
\Omega_\mathrm{r} = (2A_2 + 4A_4\phi_0^2)\sin(Q)\sin(q) - 4A_6\phi_0^2\sin(Q)\sin(2q). \qquad (3.8)
$$

The general solution of the system of equations (3.3) initially formulated in equation (3.4) will appear as a superposition of terms having the time dependence $\exp(\mathrm{i}\Omega_m t)$ and $\exp(-\mathrm{i}\Omega^*_m t)$, where the Ω_ms, with $1 \leqslant m \leqslant 4$, are the frequencies of the modulation wave relative to the extended nonlinear spin wave. The stability of the extended nonlinear spin wave is determined by the imaginary part of Ω_m given in equation (3.7). However, here we need to emphasize that, as far as the roots of the polynomial given in equation (3.6) are concerned with the present study, the modulational instability (MI) phenomenon of the extended nonlinear spin wave occurs when one of the four elements of the imaginary part of the noise's frequency is non-nil, i.e. $\Omega_\mathrm{im} = \mathrm{Im}\{\Omega_m\} \neq 0$, otherwise it is stable only if the imaginary part of the frequency vanishes. This MI is set up by an exponential growth of the amplitude of the

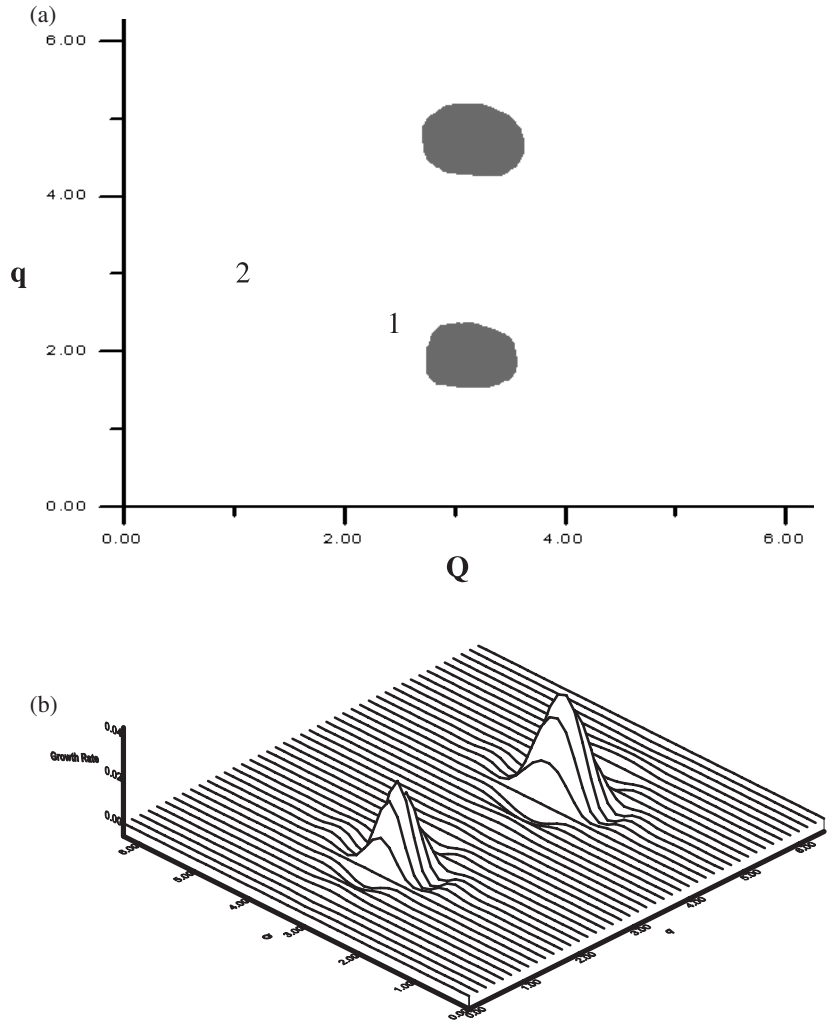

Figure 1. (a) A typical plot of regions of modulational instability in the (Q, q) plane. The black regions correspond to the unstable region while the other region corresponds to the stable region. (b) Three-dimensional plot of the growth rate of modulational waves as a function of both the wavevector of the carrier wave and the perturbation wave. The biquadratic parameter is $\alpha = 0.06$.

perturbation. Since the lattice is discrete, wavenumbers q and Q that differ by 2π correspond to the same wave. Thus, our study will be restricted to $[0, 2\pi]$ both for the carrier and for the perturbation wavenumbers. Based upon the roots of equation (3.6), which is related to the dispersion relation, the results obtained for the stability diagram can be obtained either by the analytical solutions or numerically solving equation (3.6) and the result would be the same. But the stability diagrams result presented here are obtained by numerical computation. With the above established criteria, the main features of the instability are highlighted in figure 1(a) where the stability diagram is plotted in a (q, Q) plane. In this figure, the two regions that are dark correspond to the regions of instability in which the amplitude of any wave would be expected to suddenly display an exponential growth. The corresponding growth rate is depicted in figure 1(b) as a function of the wavenumber Q of the noise by single bump with

different size for different values of the wavenumber q of the carrier. In this instability region, for a given carrier wavevector q, although the growth rate as function of the noise wavenumber has the same shape. i.e. a single bell, it remains a fact that there exist wavenumbers q for which the growth rate attains a greater value than on the other shapes. The other region, which is not dark, corresponds to the stability zone with a growth rate that vanishes. According to figures 1(a) and (b), a carrier wave with either a short wavelength or a long wavelength would be stable to any perturbation wave with any wavelength provided that its amplitude remains smaller than that of the carrier wave, but in the case of a carrier wave with approximately medium wavelength one should take care of the wavelength of the modulating wave.

4. Numerical experiments

The results presented in the previous section were deduced from a linear stability analysis. But as is well known, this linear stability analysis seems to be limited because it can only detect the onset of instability, and does not tell us anything about the behaviour of the system when the instability grow after a long time. This is why, in this section, we present the results of a numerical experiment in a discrete ferromagnetic chain. Following this, the validity of the analytical result obtained from the linear stability analysis of the extended nonlinear waves is discussed for various biquadratic exchange parameters. The influence of the anisotropy on the stability is also discussed. We will also investigate the dynamics of the different patterns of the nonlinear wave that can propagate under modulation in such a discrete magnetic chain. For this purpose, we are going to solve numerically the set of coupled nonlinear differential-difference equations of motion that would be derived from equation (2.8*b*).

4.1. Computer-simulation details

Our numerical calculations have been done through a computer-simulation program in order to make contact with the analytical prediction at short time as well as to examine longer-time dynamics of the nonlinear system which is subject to MI of the extended spin wave. For this purpose, molecular dynamics are used and we start with the dynamics of cyclic magnetic chains of 128 and 256 spins that are simulated, using a fourth-order Runge–Kutta algorithm.

We have introduced, as an example, the following set of parameters of the $CsNiF_3$ structure, namely [7] $J = 23.6$ K, $A = 9$ K and $S = 1$. In addition, working with the cyclic magnetic chain means that we chose periodic boundary conditions.

As far as equation (2.8*b*) is concerned with the description of the subsequent time evolution of the nonlinear spin-wave excitations, the origin of the energy scale of our discrete ferromagnetic chain is chosen from the uniform ferromagnetic state. Its dimensionless form is given in terms of the wavefunction and its complex conjugate for the boson mode at different lattice sites by $E = \sum_{n\rho} E_{n\rho}$, with

$$\begin{aligned} E_{n\rho} = {} & e_1|\psi_n|^2 + e_2|\psi_{n+\rho}|^2 + e_3(\psi_n\psi^*_{n+\rho} + \psi^*_n\psi_{n+\rho}) + e_4|\psi_n|^4 + e_5|\psi_{n+\rho}|^4 \\ & + e_6(|\psi_n|^2 + |\psi_{n+\rho}|^2)(\psi_n\psi^*_{n+\rho} + \psi^*_n\psi_{n+\rho}) \\ & + e_7|\psi_n|^2|\psi_{n+\rho}|^2 + e_8(\psi^2_n\psi^{*2}_{n+\rho} + \psi^{*2}_n\psi^2_{n+\rho}); \end{aligned} \tag{4.1}$$

here, the coefficients e_i *with* $i \in (1, \ldots, 8)$ are expressed in the appendix.

With a suitable choice of the time step, this energy is a conserved quantity. It was frequently monitored in our simulations to insure an accuracy of about 0.1% for the fourth-order Runge–Kutta scheme.

The initial conditions, which are typically at time $t = 0$, initial profiles of the spin deviation are obtained by using a complex wavefunction that can be written as

$$\psi_n(t) = \psi_n^{\mathrm{re}}(t) + \mathrm{i}\psi_n^{\mathrm{im}}(t). \tag{4.2}$$

Here, the upper indices (re) and (im) stand for the real and the imaginary part, respectively. We start from a solution of the discrete nonlinear equation (2.8*b*) as a plane wave of wavevector q with an amplitude which is perturbed by a modulation plane wave with wavevector Q since we are interested in modulational instability. Thus initially, in our numerical simulation, the real and the imaginary part of the wavefunction of the spin wave are coherently modulated in the form

$$\psi_n^{\mathrm{re}}(0) = (\phi_0 + \eta\cos(nQ))\cos(nq) \tag{4.3a}$$

$$\psi_n^{\mathrm{im}}(0) = (\phi_0 + \eta\cos(nQ))\sin(nq). \tag{4.3b}$$

This initial condition is therefore a modulated plane wave with amplitude ϕ_0 that is the same parameter as the one of the preceding section and the modulation amplitude $\eta \ll \phi_0$. In our simulation, the wavenumbers $q(Q)$ are defined modulo 2π in the lattice and chosen in the form $q = \frac{2\pi p}{N}$ ($Q = \frac{2\pi P}{N}$), where $p(P)$ is an integer. So, using the initial condition given in equations (4.3) has revealed that in this simple coherent modulation form of the amplitude this initial condition allows us to study the response of the system separately for each modulation wavevector.

4.2. Numerical-results

Once the initial conditions of equations (4.3) are given, the time evolution of a modulated spin wave can be investigated by means of the above-mentioned molecular dynamics (MD) simulations. In order to monitor the time evolution of individual Fourier components, we define the complete spatial Fourier transform of the wavefunction.

$$m(p,t) = \sum_{n=0}^{N-1} \psi_n(t)\mathrm{e}^{\mathrm{i}(2\pi np/N)}, \qquad \text{with } 0 \leqslant p \leqslant N/2. \tag{4.4}$$

Notice that in equation (4.4), $\psi_n(t) = \langle a_n(t)\rangle$ is the expectation value of the magnon operator, which is proportional to the transverse value of the precessing magnetization $M^+ = M_x + \mathrm{i}M_y$ and thus represents a spin-wave amplitude [42].

4.2.1. Stability for short time. For specific examples, we first consider a chain of 128 spins, keeping in mind that periodic boundary conditions are used. The biquadratic parameter is taken to be $\alpha = 0.06$ and the amplitude $\phi_0 = 0.25$. Figure 2(a) shows the evolution of a carrier wave with wavevector $q = 35\pi/64$ modulated by a small-amplitude wave ($\eta = 0.0025$), with wavevectors $Q = \pm 52\pi/64$, for about 500 units of time. According to figure 1(a), stability is predicted for waves with these wavenumbers. This is effectively verified numerically in the log–linear plot of figure 2(a), in which none of the $q \pm Q$ satellite side bands display any exponential growth. Even the $2q$ modulation, which is not taken into account in the initial conditions, displays constant amplitude. Figure 2(b) shows the complete Fourier spectrum on which we can observe that the stability predicted in figures 1(a) and (b) is numerically verified. The same verifications of the stability of waves based upon the results of figure 1(a) can be done with this timescale and physical parameters but with different wavenumbers, provided that the wavenumber of the perturbation does not fall in the instability zone.

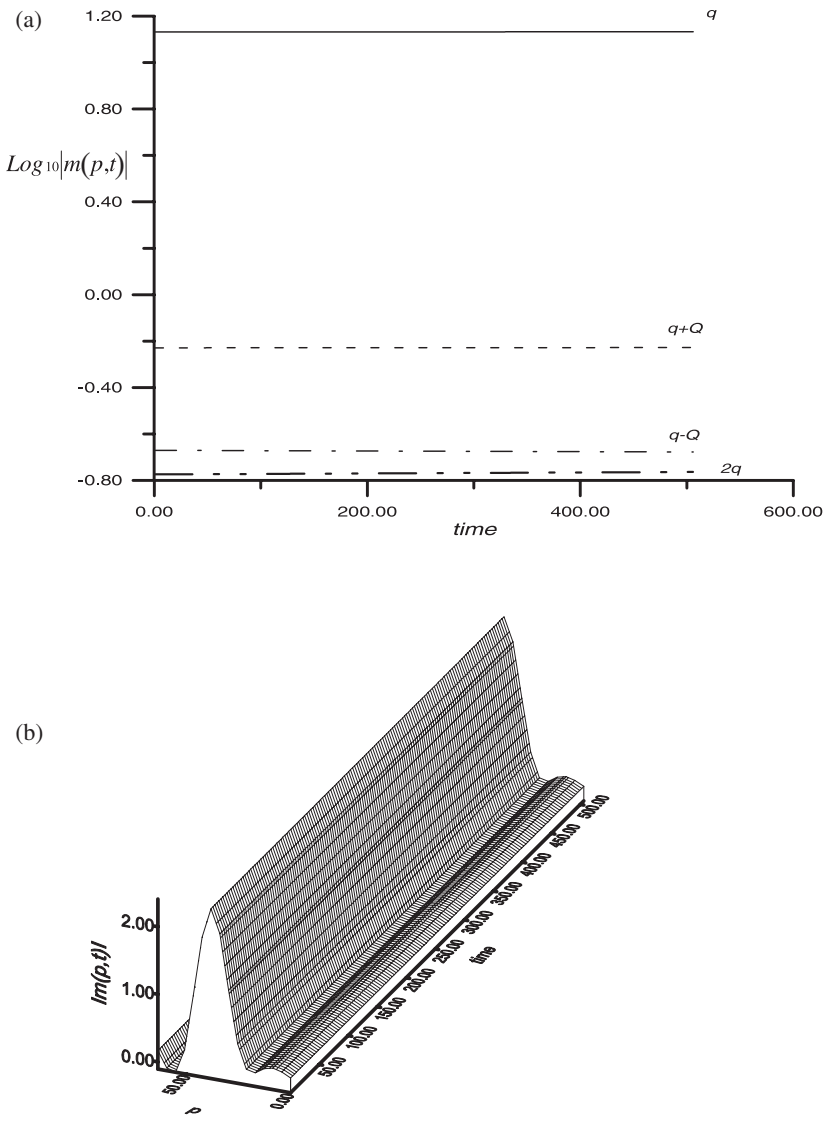

Figure 2. Time evolution of the carrier wave with $q = 35\pi/64$ and $\phi_0 = 0.25$ modulated by a small-amplitude wave with $Q = 52\pi/64$ and $\eta = 0.0025$. (a) Time evolution of the amplitude of the main Fourier transform components at q (solid line), $q + Q$ (dashed curve), $q - Q$ (dot–dashed curve) and $2q$ (dot–dot–dashed curve). A logarithmic scale is used for the ordinate. (b) Time evolution of the complete Fourier spectrum.

4.2.2. Stability for long time and influence of the biquadratic exchange interaction and the anisotropy. If the duration of the simulation is very long, the first result that may be surprising at a first glance is that, contrary to what is obtained in previous works on MI processes [33, 45, 47] (to cite a few), the prediction of stability from linear analysis seems to rule out the occurrence of instability if the biquadratic parameter is in the range $\alpha \leqslant 0.5$. The reason for this predictability is that, even if there is a presence of higher harmonics and their combinations that is neglected at the initial step of the simulation, in the outcome of the simulation, all the time, all the wavenumbers of the higher harmonic would fall outside the

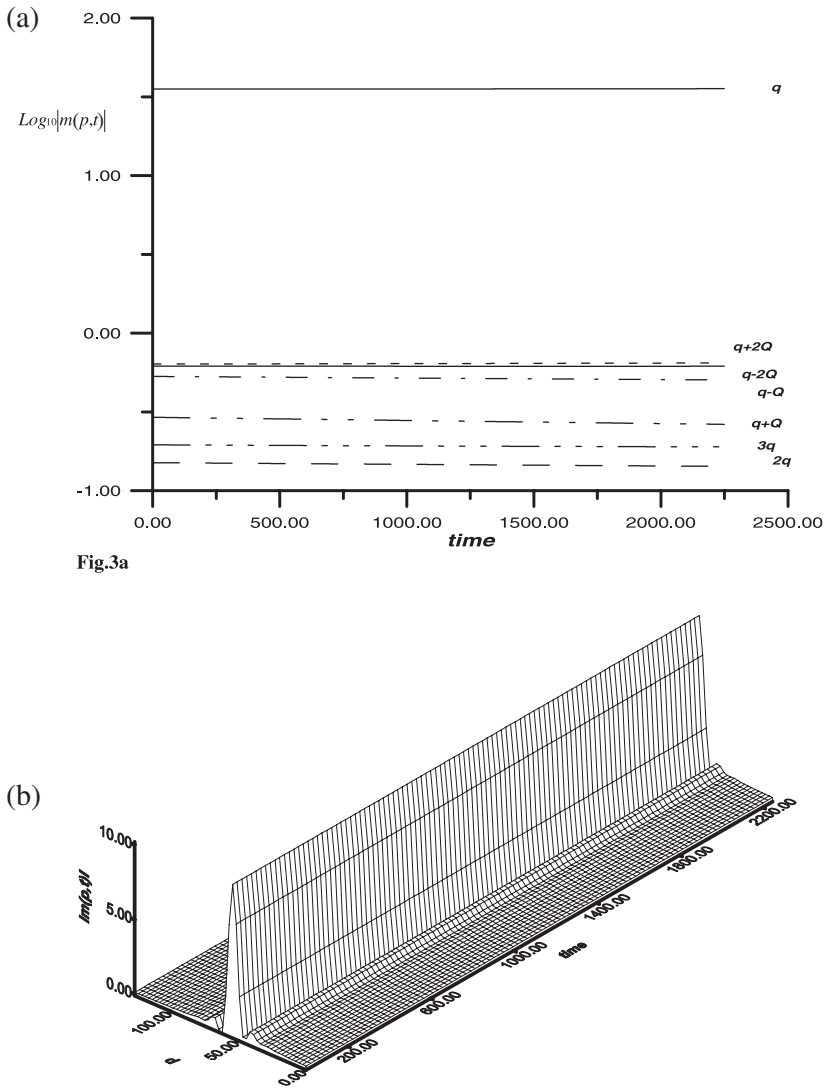

Fig.3a

Figure 3. Time evolution of the carrier wave with $q = 27\pi/64$ ($p = 54$) and $\phi_0 = 0.15$ modulated by a small-amplitude wave with $Q = 61\pi/64$ ($P = 122$) and $\eta = 0.0015$. (a) Time evolution of the amplitude of the main Fourier transform components at q (solid line), $q + 2Q$ (dashed curve), $q - 2Q$ (second solid line), $q - Q$ (dot–dashed curve), $q + Q$ (dot–dot–dashed curve), $3q$ (dot–dot–dot–dashed curve); the second dashed line is for the $2q$ modulation. The biquadratic parameter is $\alpha = 0.06$. A logarithmic scale is used for the ordinate. (b) Time evolution of the complete Fourier spectrum.

instability zone. Consequently, none of the different mode displays any growing behaviour. We explain this special feature by the fact that, first, the regions of instability have very small size; and second, in this range of wavenumbers, these simulations confirm the prediction of the stability when a modulated wave moves in the spin chain with a vanishing imaginary part of the frequency of the modulating wave. To illustrate this point, the long-time evolution of a perturbed wave with wavevector $q = \frac{27\pi}{64}$ ($p = 54$) in a ferromagnetic chain of 256 spins is plotted in figure 3(a). In this case, the modulation wavevectors $Q = \pm\frac{61\pi}{64}$ ($P = 122$) also

lie in the stable region as can be verified in figure 1(a). Here, the biquadratic parameter is chosen to be $\alpha = 0.06$, that is a best value for the stability for a very long-time evolution of the modulated waves. With the thus-chosen parameters, we observed in figure 3(a) where the main feature of the stability is depicted that even though there is a presence of other harmonics that have a very small and constant amplitude for long time, the main carrier wave time evolution is also stable for a very long time. We also notice the presence of not only the principal $q \pm Q$ satellite modulations that are considered in the initial condition, but also the presence of other combination modes $2q$, $3q, \ldots$ and also $q \pm 2Q$. The other higher harmonics even if they are not presented here also display constant amplitude but with smaller magnitude than that of the $3q$ modulation. The magnitude of the modes generated decreases with increasing of the harmonic order. In this case, we can attest that the discrete ferromagnetic chain can support long-lived excitations in the presence of low-amplitude noise with suitable wavenumbers. Furthermore, it is possible with our approach of modulational instability to create localized excitations or a string of localized excitations in a discrete ferromagnetic chain. This apparent phenomenon can be expected because of the fact that the lattice is discrete. Therefore, in such a condition the lack of continuous translational symmetry would lead to a trapping of the pulses generated by the nonlinear instability, by the discreteness effects, to finally form strong localized or a string of strong localized long-lived excitations. Figure 3(b) shows the time evolution of the complete spectrum where, due to the constant behaviour and the smaller magnitude of the other Fourier component compared to that of the carrier wave, the additional combination modes generated from wave-mixing processes cannot be seen in this spectrum. Notice that for these simulations we used a timescale with $t = \frac{2T_{\mathrm{SWF}}}{JS}$. i.e. $t \approx \frac{2T_{\mathrm{SWF}}}{25}$ as the unit of time. Here T_{SWF} denotes the period of the spin wave of a ferromagnetic chain that can be derived from the frequency given in the dispersion relation of equation (3.2) in the case of the low-amplitude and long-wavelength approximation. This said, the long-time simulation observed in the result of figure 3(a), which shows that the modulated wave is stable over the entire time range investigated corresponding to 2200 units of time, is about 176 periods of a carrier at spin-wave frequency.

Nevertheless, it is also possible to obtain the instability if the wavenumbers of the noise fall in the instability zone. To illustrate this point, we present in figure 4(a) the complete Fourier spectrum of the full time evolution of a carrier wave with wavevector $q = \frac{44\pi}{64}$ modulated by waves with wavevectors $Q = \pm\frac{61\pi}{64}$ that lie in the instability zone. The physical parameters here are the same as those of figures 3(a) and (b). We observe in this figure that initially the amplitude of each mode increases slowly with increasing time because of the low value of the growth rate. However, after about 800 units of time (64 periods of spin waves) all the different modes and combination modes suddenly display a large increasing behaviour of their amplitudes. This is the proof that at this timescale the system is completely unstable. But in order to understand what happens in this unstable zone we depict in figure 4(b) the time evolution of some principal modes. In this figure it is realized that, although the amplitude of most of the Fourier component of the different modes initially increases with a small rate, the $3q$ modulation is the one that rapidly seeds the instability process in the system. This can be understood by the fact that its magnitude increases with a higher rate than all the other modes. This is also the proof that, although the linear-stability analysis neglects additional combination mode waves generated though wave-mixing processes, these, albeit small at the initial stage, can become significant and drive the system into a chaotic regime at large timescale if its wavevector falls in an unstable domain.

Plotted in figures 5(a) and (b) are the stability diagram and the corresponding growth rate, respectively, for $\alpha = 0.7$. From these figures, we realize that the instability regions are larger and that the maximal size of the growth rate had increased, compared to those of figures 1(a)

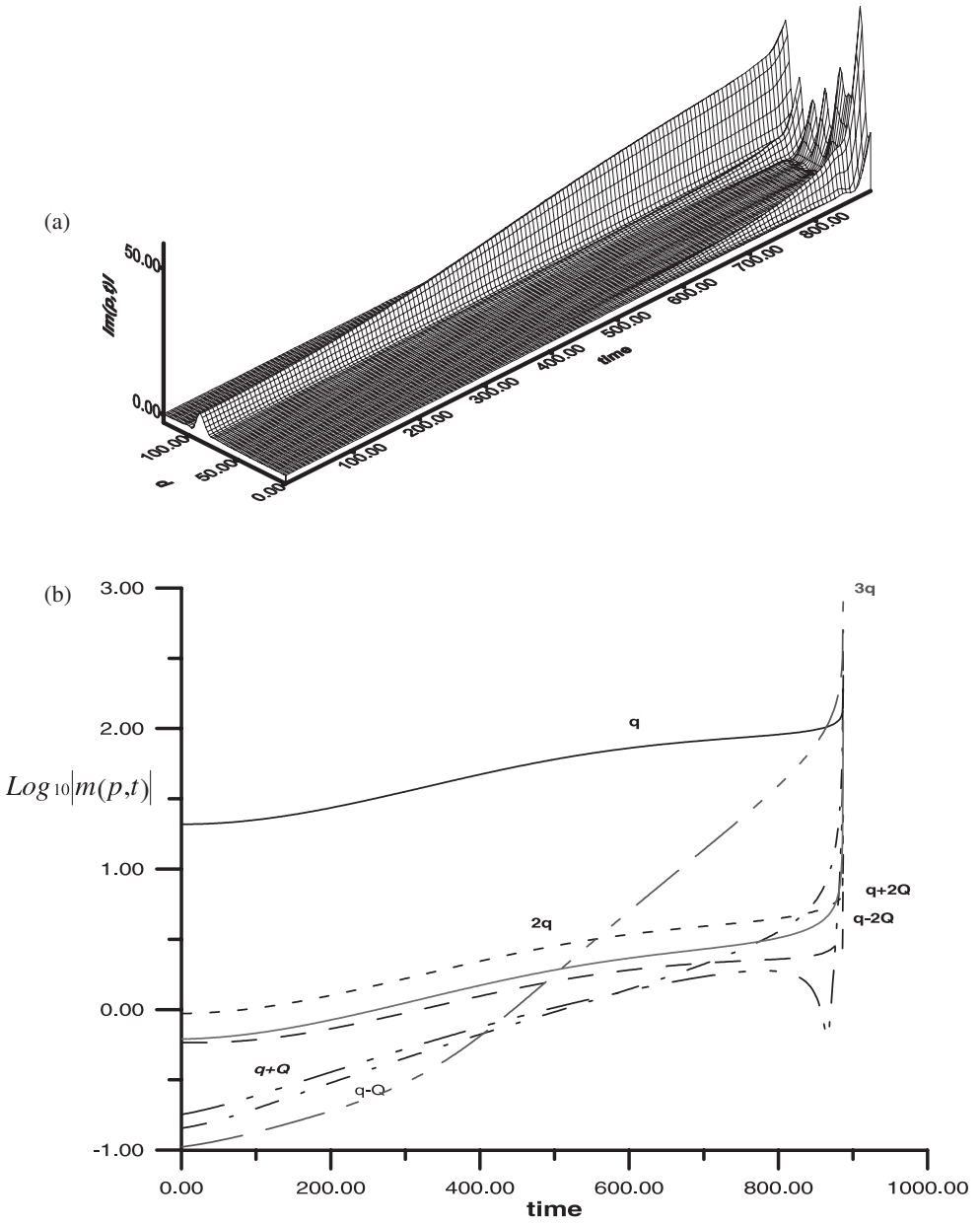

Figure 4. Complete spectrum of the time evolution of the carrier wave with $q = 44\pi/64$ and $\phi_0 = 0.12$ modulated by a small-amplitude wave with $Q = 61\pi/64$. (b) Time evolution of the amplitude of the main Fourier transform components at q (solid line), $q - Q$ (dashed–dot–dashed curve), $q + Q$ (dashed–dot–dot–dashed curve), $2q$ (dashed curve), $q + 2Q$ (second solid curve), $q - 2Q$ (second dashed curve) and $3q$ (dashed–dashed–dot–dot–dot–dashed–dashed curve) modulation.

and (b), respectively. Thus, materials for which the biquadratic interaction is higher than the anisotropy interaction would be likely to show a strong modulational instability. Moreover, for higher values of the biquadratic exchange parameter (i.e. $\alpha > 0.5$), our simulations show

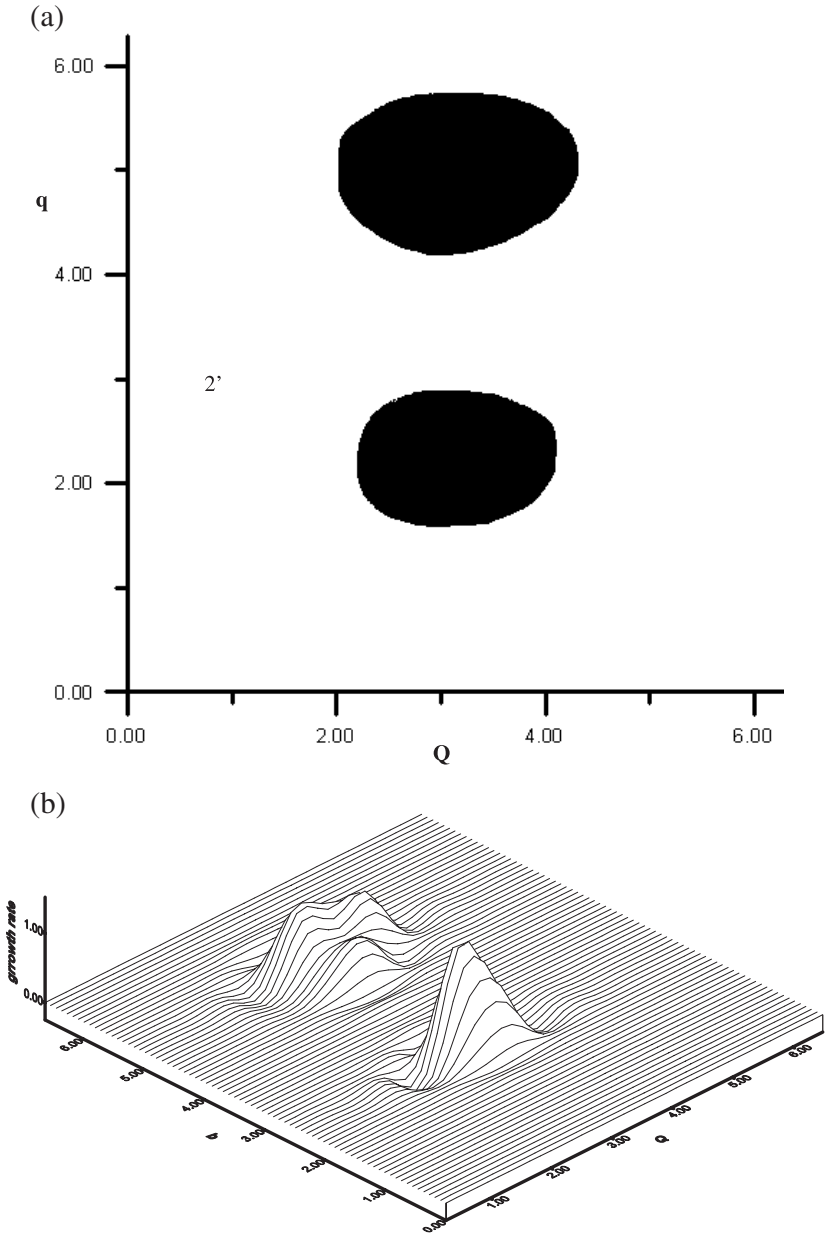

Figure 5. (a) A typical plot of regions of modulational instability in the (Q, q) plane for the biquadratic parameter $\alpha = 0.7$. The dark regions correspond to the unstable region while the other region corresponds to the stable region. (b) For the same value of the biquadratic parameter, depicted here is a three-dimensional plot of the growth rate of modulational waves as a function of both the wavevectors of the carrier wave and the perturbation wave.

that waves which are predicted to be linearly stable for the smallest value of α (i.e. $\alpha < 0.5$) can become unstable. The reason for this unpredictability is due on one hand to the size of the instability region that increases, and on the other hand the principal Fourier component falls in the instability domain and higher harmonics and their combination that are neglected at the

initial step of the simulation appear with an exponential growth. To justify this argument let us choose for instance the point labelled by (1) in figure 1(a), which corresponds to the point with $q = \frac{45\pi}{64}$ ($p = 90$) and $Q = \frac{57\pi}{64}$ ($P = 114$). In figure 1(a) this point corresponds to a stable point; a simulation of the long-time evolution of a perturbed wave with wavenumbers corresponding to this point would lead to the similar results as those of the case of figures 3(a) and (b). In figure 5(a) for which $\alpha = 0.7$ this point is in the instability zone and thus any time evolution in Fourier space of a perturbed wave with the corresponding wavenumbers would lead to similar results as those of figures 4(a) and (b). Furthermore, let us depict in figure 6(a) the time evolution of a perturbed wave, with wavevector $q = \frac{15\pi}{32}$ in a ferromagnetic chain of 256 spins. In this case, the modulation wavevectors $Q = \pm\frac{15\pi}{64}$ lie in the stable region in the point labelled by (2′) as can be verified in figure 5(a); its corresponding point in figure 1(a) is labelled by (2). Here, the biquadratic exchange parameter is chosen to be $\alpha = 0.7$. With the thus-chosen parameters, we observe in figure 6(a) that, even though there is a presence of other harmonics, the main carrier wave time evolution is stable for a very long time. We notice the presence of the satellites at $q \pm Q$ modulations that are considered in the initial condition, and also that of other combination modes $2q, 3q, \ldots$ and $q \pm 2Q$ that are progressively generated in the system. The other higher harmonics even if they are not presented here also display constant amplitude but with smaller magnitude than that of the $3q$ modulation. This magnitude would decrease with increasing of the harmonic's order. In this case, the $2q$ mode can be obtained by the combination of a q mode with $2Q$ modulation. One of the most important results while looking at figure 6(a) is the behaviour of the other modes. Their amplitudes display an increasing behaviour with increasing time, but with a very low rate such that their magnitudes remain very small compared to that of the carrier wave component. Finally, in this case, even if the other modes display a slight increasing behaviour, they do not increase up to significant values. Therefore the prediction of stability remains likely. In figure 6(b), we have plotted the complete Fourier spectrum in which, due to the smaller values of the magnitude of the other harmonics generated by wave-mixing processes compared to that of the carrier wave, no apparent modulation is seen.

Needless to mention, these simulations demonstrate that, for a given ferromagnetic material, if the strength of the biquadratic exchange interaction is smaller than or at least close to that of the crystal anisotropy field, i.e. the parameter α fulfils $\alpha \leqslant 0.5$, the physical system can support very long-lived excitations that are excited by MI processes. However, if the strength of the biquadratic interaction is higher than that of the crystal field anisotropy (i.e. $\alpha > 0.5$), even if the physical system can still support excited carrier waves in a reduced zone of stability, it is clear that they would finally be destroyed by instability processes if the biquadratic parameter is further increased. This can be understood by the fact that, for small values of the biquadratic exchange parameter, the combination modes at $q \pm 2Q, q \pm 3Q, \ldots$ generated by wave-mixing processes induced by the nonlinearity appear initially with lower amplitude than that of $q \pm Q$ by at least a factor of β, and still lie in the stable region after a very long time. Even the $3q$ modulation that appears initially with a greater amplitude than that of the $q \pm Q$ satellite still lies in the stable zone after a long time. Meanwhile, in the case of the highest values of the biquadratic exchange parameter, the largest region of instability occurs, and therefore, even if the growth rate is small, the amplitude of the combination modes would increase up to very significant values and it may drive the system into a chaotic regime, when carrier waves fall in instability regions. Thus, in this latter case the combination modes would play an important role at any timescale. Hence, from the result presented in figures 3(a) and (b), 4 and 6(a) and (b), it is realized that not only the main satellite modulation but also all combination modes must not lie in the regions of instability. Notice that, like in the other models such as the Klein–Gordon lattice and the Fermi–Pasta–Ulam lattice, the nonlinearity in the

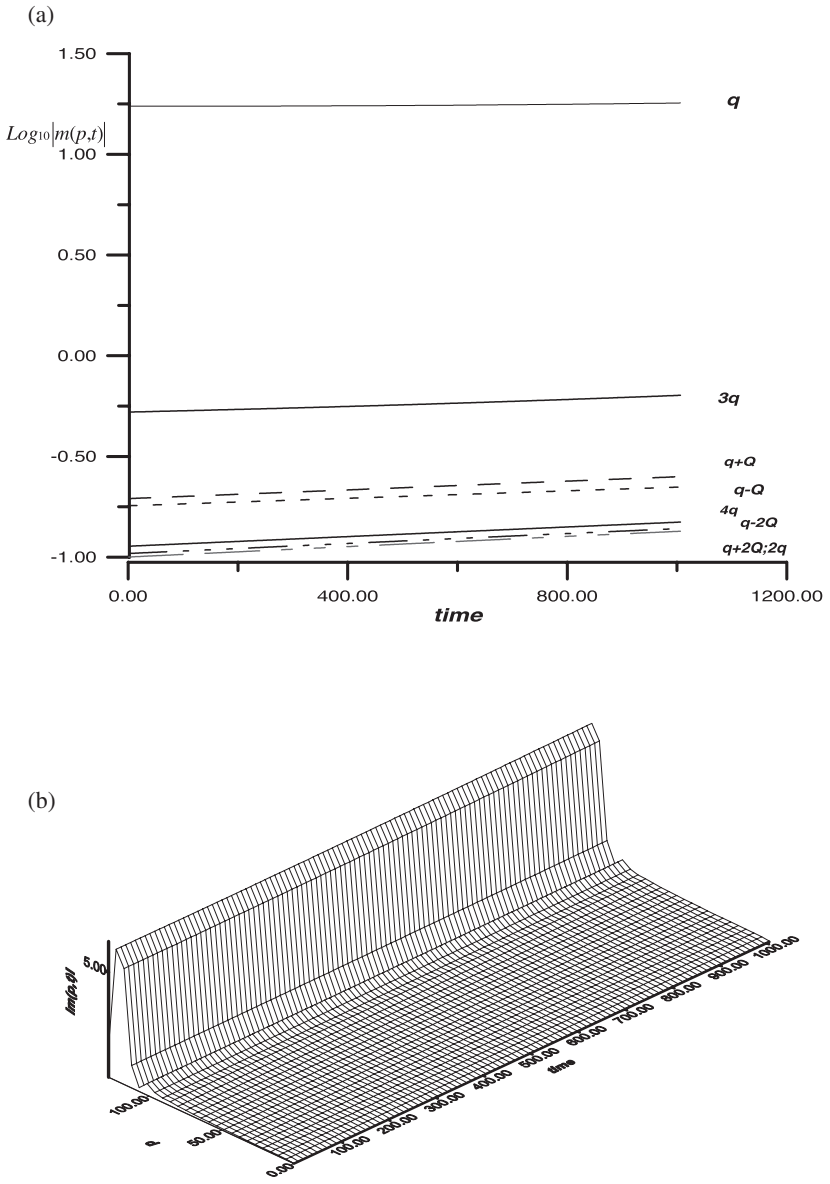

Figure 6. Time evolution of the carrier wave with $q = 15\pi/32$ and $\phi_0 = 0.12$ modulated by a small amplitude wave with $Q = 15\pi/64$, plane for a value of the biquadratic parameter $\alpha = 0.7$. (a) Time evolution of the amplitude of the main Fourier transform components at q (solid line), $q + Q$ (first dashed curve), $q - Q$ (second dashed curve), $2q$ or $q + 2Q$ (dashed–dashed–dot–dot–dot–dashed–dashed curve) and $q - 2Q$ (dashed–dot–dot–dot–dashed curve); the second solid line is for the $3q$ mode. The third solid line is for the $4q$ modulation. A logarithmic scale is used for the ordinate. (b) Time evolution of the complete Fourier spectrum.

uniaxial easy-axis ferromagnetic chains also generates combination waves at $\pm 2q, \pm 3q, \ldots$, etc. With the periodicity of an equivalent size of Brillouin zone taken into account (i.e. $[0,\ 2\pi]$ for the wavenumbers), the stability condition is given by

$$\mathrm{mod}(\pm nq,\ 2\pi) \notin \text{ unstable regions for } n > 1, \tag{4.5a}$$

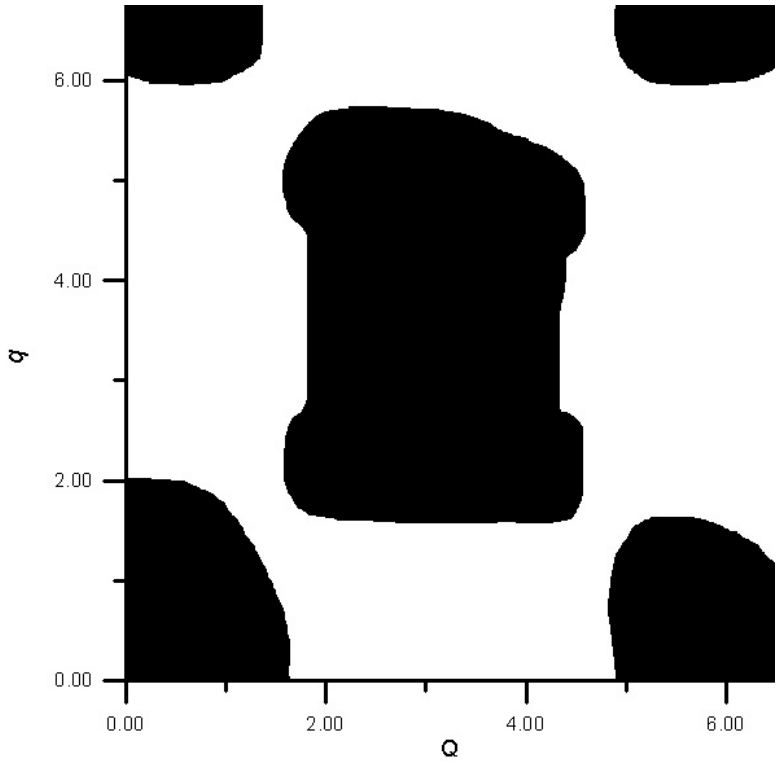

Figure 7. A typical plot of regions of modulational instability in the (Q, q) plane for the biquadratic parameter $\alpha = 0.95$ and $\phi_0 = 0.45$. It is obvious that with increasing of the biquadratic parameter and the amplitude of the initial condition, the dark regions where the instability occurs are enlarged while the other region corresponding to the stable region is reduced.

and

$$\mathrm{mod}(q \pm nQ,\ 2\pi) \notin \text{ unstable regions for } n = 1, 2, \ldots. \tag{4.5b}$$

According to the above criteria, a 1D ferromagnetic chain can be seen as a 1D atomic chain.

As the biquadratic exchange parameter increases, the ferromagnetic chain appears to be less anisotropic, and according to analytical results the area of the instability regions in the (Q, q) plane also grows so that the two former regions of instability recover each other and new regions of instability can even appear. To illustrate this point, we have plotted in figure 7 the case of $\alpha = 0.95$ with the amplitude of the initial condition $\phi_0 = 0.45$. In this condition, the size of the instability region becomes very sensitive to a slight variation of the amplitude of the initial carrier wave. In this figure, it is obvious that with increasing of the biquadratic exchange parameter and the amplitude of the initial condition the dark regions where the instability occurs are enlarged and also new regions of instability appear in the boundaries, while the other region corresponding to the stable region is reduced.

To illustrate the effect of the anisotropy on the stability of all the excitations that may arise in the framework of this study, we have plotted in figures 8(a)–(c) the stability diagram with different values of the anisotropy parameter. Before we start this investigation it is worth mentioning that the results presented in figures 1(a), 5(a) and 7 correspond to the case of the $CsNiF_3$ material, i.e. with the same anisotropy parameter $A/J = 0.382$. While looking at figure 8(a), that corresponds to the case with the same biquadratic parameter as that of figure 1(a) but with

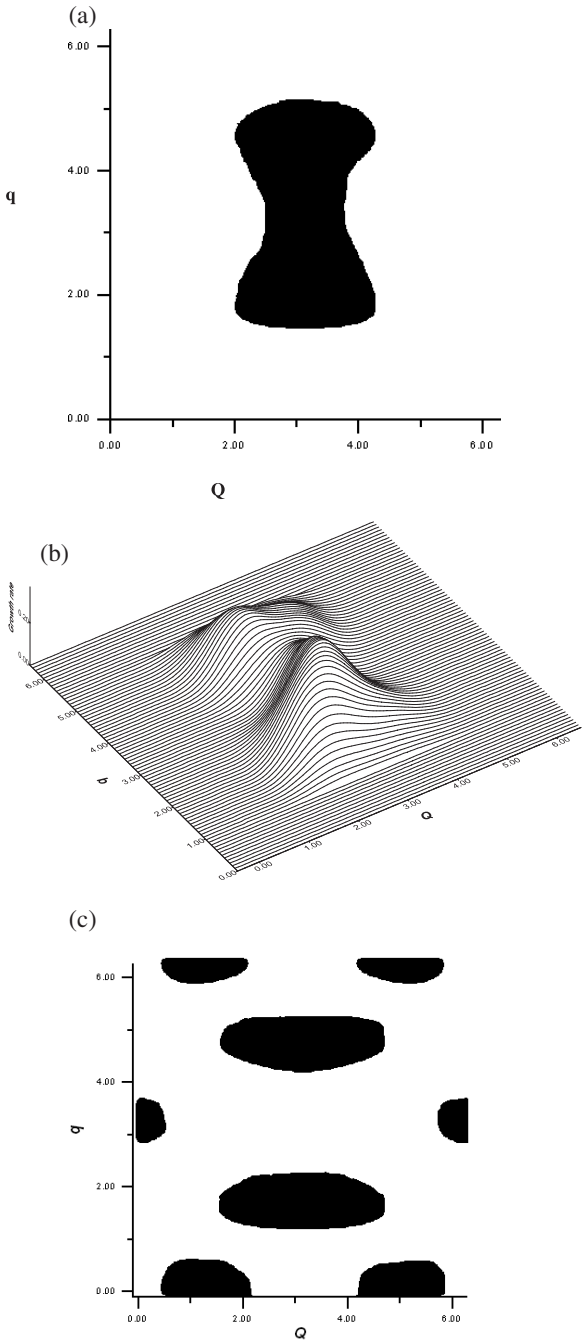

Figure 8. A typical plot of regions of modulational instability in the (Q, q) plane showing the influence of the anisotropy parameter on the stability/instability region (a) for the biquadratic parameter $\alpha = 0.06$ and $\phi_0 = 0.12$ (the same as in figure 1(a)) and the anisotropy parameter different from that of figure 1(a) i.e. $A/J = 1.52$. (b) The corresponding growth rate with the same physical parameters as those of figures 8(a) and (c) for the biquadratic parameter $\alpha = 0.95$ and $\phi_0 = 0.45$ (the same as in figure 7) with the anisotropy parameter different from that of figure 7. i.e. $A/J = 0.95$.

the anisotropy parameter $A/J = 1.52$, it is realized that increasing the anisotropy parameter leads to an increase of the size of the instability zone. However, even though the unstable zone slightly increases with the wavevector of the modulating wave, this increasing behaviour occurs more with the wavevectors of the carrier wave situated within the range of the wavevectors of the two initial unstable zones of figure 1(a). Thus, the two initial unstable zones finally recover each other and it turns out that the system displays only one unstable zone that may continue increasing. We also noted that reducing the anisotropy parameter may reduce the instability zone. But what appears as a surprising behaviour is that the instability zone does not disappear completely even with the anisotropic parameter which is nil. This is understandable from the fact that the anisotropy only appears in two coefficients, A_1 and A_3, of equations (2.8*b*) (see the appendix). Therefore, annealing the anisotropy in this model does not cancel the different coefficients of the equation of motion. Hence, the instability persists even with an isotropic model. Although figures 8(a) and (b) correspond only to the biquadratic parameter of figures 1(a) and (b), we noticed the same type of influence of the anisotropy on the instability zone with most of the other greatest values of the biquadratic parameter. The only peculiar behaviour occurs when the anisotropy parameter and the biquadratic parameter are equal and therefore cancel the coefficient A_3 of the discrete nonlinear Schrödinger-like equation (2.8*b*) i.e. $A_3 = 0$. To illustrate this point, we plotted in figure 8(c) the case with the same value of the biquadratic parameter as in figure 7 but with an anisotropy parameter that take the same value of the biquadratic parameter. While looking at figure 8(c) it is realized that, contrary to what is observed in figure 7, the stability persists in the region of wavevectors lying between the two initial unstable zones. But the increase of the instability zone in this diagram occurs more with the appearance of the new unstable regions in the system. From figure 8(c) it can be understood that materials for which the biquadratic parameter and the anisotropic parameter are equal would tend to display instability of a linear excitation of the carrier wave with some wavevectors that are modulated with a small-amplitude wave with both short wavelength and long wavelength. In the case of materials that display different values between the anisotropy and the biquadratic parameter, if the anisotropy is less than that of the $CsNiF_3$ material, the system would be more likely to display stable excitations constituted with a linear carrier wave modulated in its amplitude. In the case of materials with higher anisotropy than that of $CsNiF_3$, they would display instability of modulated waves with any wavelength because of the increasing behaviour of the instability zone with increasing anisotropy. Thus, the wavevector of the modulating wave would easily fall in the unstable zone.

5. Spin-wave pattern formation in ferromagnetic chains

It was demonstrated some years ago that in one-dimensional spin chains, at suitably low temperature, one may view thermal excitations as spin waves, supplemented by a dilute gas of thermally magnetic solitons [7]. This argument was based on the fact that, in a 1D spin chain, one may have solitons whose excitation energy is comparable to $K_B T$, because they are localized at the microscopic scale. After this particular feature of the soliton excitations in magnetic chains, new nonlinear spin excitations in 1D spin system had been discovered and to date it remains an active research topic [28, 29]. These excitations have envelope functions with shape familiar from the theory of soliton-like objects, but in contrast to the solitons they emerge as solutions of the time-dependent classical equations of motion. Furthermore, when such an entity is present, each spin in the system engages in circular precession, with a frequency that lies outside the spin-wave band. These states are the magnetic analogues of the intrinsic anharmonic localized modes discussed very actively in the literature on the vibrations of 1D anharmonic atomic chains [43]. Up to now, although some effort had been

made to understand how to excite these new nonlinear localized magnetic excitations [44], their possible role in the thermodynamics remains unclear. However, determining whether the new nonlinear wave generated by MI can lead to localized excitation is still an open question in ferromagnetic systems.

In this section, we examine the nature of different wave pattern formation that may arise by a modulational instability process in a ferromagnetic chain described by the model of equation (2.8*b*). We then continue by using the definition of wavenumber given above (i.e. $q = \frac{2\pi p}{N}$ ($Q = \frac{2\pi P}{N}$)) of a carrier wave (of the noise), with p in the range $0 < p \leqslant N/2$, and we choose $P = 30$ to always stay in the stable domain of wavenumbers (frequencies). Reducing the range of p in the half interval of the spin lattice is linked to the fact that, after the value of $p = N/2$, we start recovering the same phenomena when increasing p up the value of N. This is explained by the symmetric property of the spin chain, which allows deduction of the different features obtained on one side of the chain from the one obtained on the other side of the same spin chain. The chain is still constituted of 256 spins and we chose the initial condition given in equations (4.3).

For values of p in the range $0 < p \leqslant 20$, when the initial condition is introduced in the chain, the wave pattern displayed by the set of precessing spins is that of a wave plane with a sinusoidal form with a constant amplitude that is not sensitive to any modulation as the time increases. Here, the number of oscillations is equal to the value of p. In this range, the spin wave is neither sensitive to the nonlinear effects of the chain nor to its discrete nature.

In the range $20 < p \leqslant 60$, while increasing p up to the value of $p = 60$, we observe that the wave pattern displayed by the precessing spins is that of a plane wave, but with the difference here that, instead of a constant behaviour, the amplitude, which appears proportional to the spatial magnetization distribution, is modulated in the form of an extended small-amplitude oscillating short wave.

When the values of p lie in the range $60 < p \leqslant 80$, one of the interesting phenomena is that, although the real or imaginary parts of the wave display an oscillating and breathing wave behaviour, the amplitude or the spatial magnetization distribution of the wave displayed by spin motion is modulated in terms of a train of small-amplitude short waves. Each element of the train has the shape of a soliton object. To illustrate this point, we present in figures 9(a) and (b) the real part as well as the amplitude of the wave pattern displayed by the precessing spins for a value of $p = 65$, in the case of figure 9(a), and $p = 66$ corresponds to the case of figure 9(b). It is clear that the value of p influences the number of the wave oscillating with soliton shape in the train. This phenomenon can be understood in the sense that, in this range of p (i.e. frequency), the nonlinear effects in the discrete spin lattice lead to the creation of an extended nonlinear spin wave with a particular fact that the amplitude appears as a train of soliton-like objects.

Further increasing the value of p up to the range $80 < p \leqslant 90$, we realize that there appears a modulation both in the amplitude and the imaginary part as well as in the real part of the wavefunction displayed by the spin motion. Here, the amplitude and the real and imaginary parts appear as an extended short wave moving with breather properties. Thus, the wave pattern displayed here is that of an extended wave that propagates with a breathing motion. This phenomenon is depicted in figure 10, for $p = 85$, where the real part of the wavefunction and its amplitude is plotted.

In the range $90 < p \leqslant 110$, it happens that the wave pattern displayed by the spin motion is constituted by an extended wave with an amplitude modulating into a train of double pulses while the real and the imaginary part of the wave modulate with period doubling compared to that of the amplitude. Here the nonlinear effects show some premixing to the formation of a particular wave train.

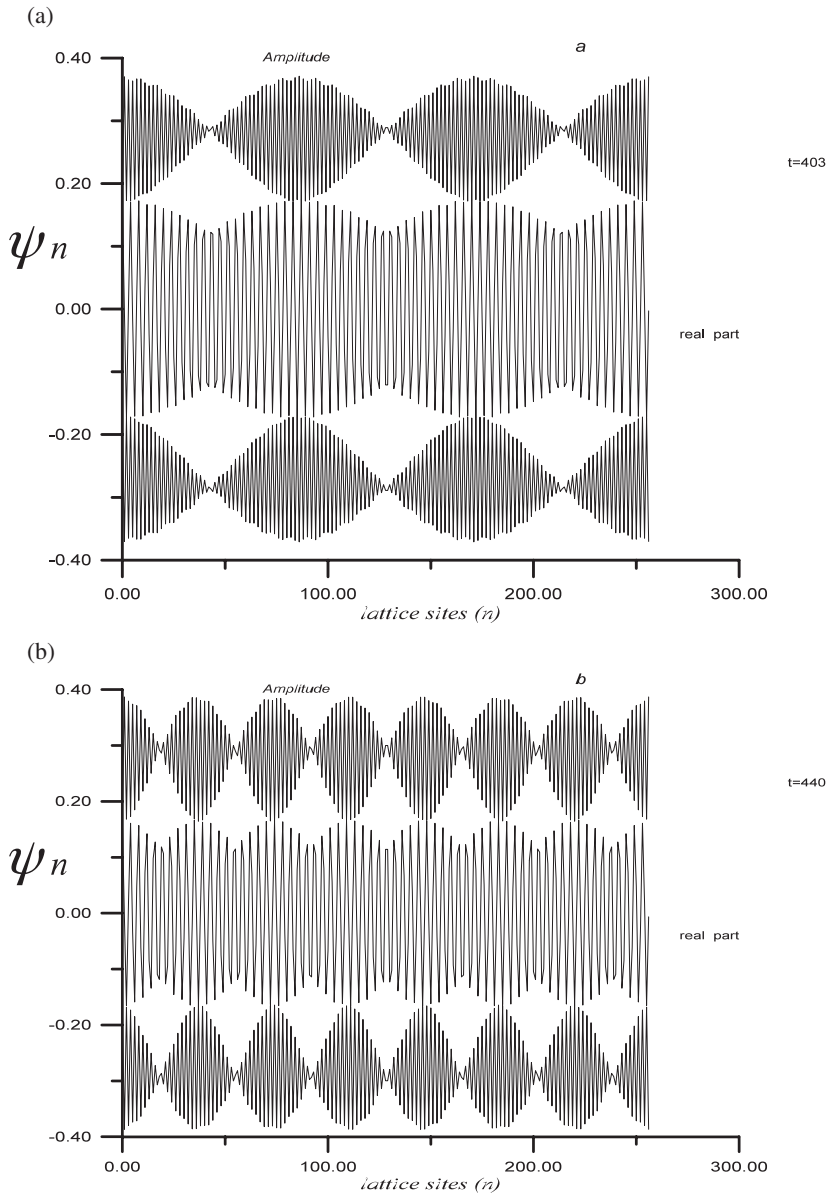

Figure 9. We show only the real part of the wavefunction $\mathrm{Re}(\psi_n)$, which is intercalated between the amplitudes $|\psi_n|$ that appear as a train of soliton-like objects. (a) The case of $p = 65$ obtained at time $t = 403$ and (b) the case of $p = 66$ obtained time $t = 440$. It is clear to see how the value of p influences the number of soliton-like objects in the chain.

If p is chosen in the range $110 < p \leqslant 127$, we observe that the amplitude and the real or imaginary part of the wave pattern constituted by the spin chain show modulation with a depth that increases with time (see figures 11(a) and (b)). Therefore, after a certain time, it turns out that the spin wave presents the form of a train of bubbles. These bubbles are constituted by an imaginary part of the wavefunction that has a soliton-object-like shape while the amplitude has a periodon-like shape. At this stage, the wave pattern of the spin chain can be

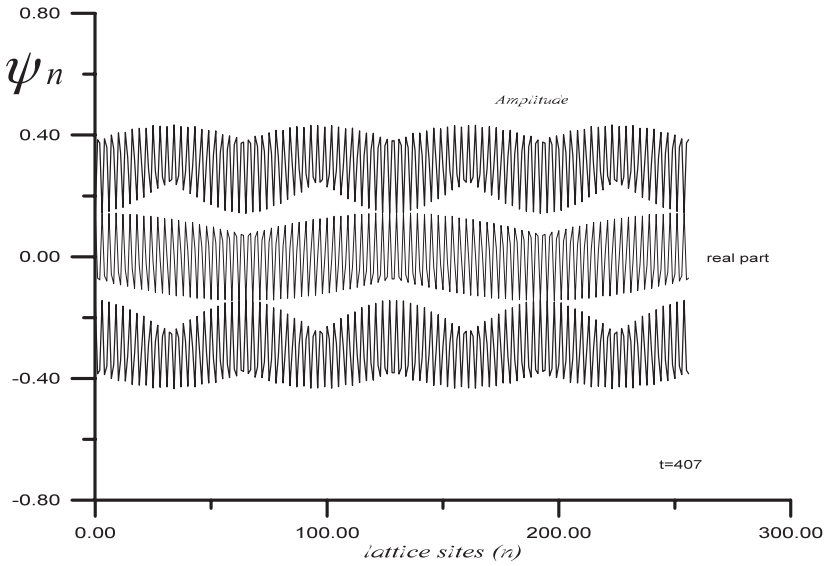

Figure 10. We show here how extended the spin wave is in the magnetic chain through the plot of the real part of the wavefunction $\mathrm{Re}(\psi_n)$, which is intercalated between the amplitudes $|\psi_n|$ that appear as an extended wave with a breathing behaviour. This is obtained for $p = 85$ at time units $t = 407$.

considered as a train of periodons (see figures 11(b) and (c)). However, if we further increase the time, the spatial magnetization distribution is transformed into a localized mode or a train of localized modes with breathing motion. For instance, here, if $p = 127$, the wave pattern will be constituted with only one localized mode that would be created on its modulated amplitude. If we decrease the value of p, the number of localized breathing modes starts increasing in the spin chain. This is the so-called intrinsic localized mode since it is produced in the Brillouin zone boundary as demonstrated by previous authors [33]. As we have emphasized in a previous section related to the result of figure 3, this can be understood in the sense that the first Brillouin zone boundary is the region where a trapping of the pulses generated by linear wave instability of the low-amplitude noisy background, by the discreteness effects, finally forms strong localized or a string of strong localized long-lived excitations. To illustrate this point we have plotted in figures 11(d) and (e) the wave pattern displayed by the precessing spin under modulation through the spatial magnetization distribution. It is then realized that, depending on the value of p (i.e. the wavenumber), MI processes can lead to the creation of a hierarchy of intrinsic localized modes on the spatial magnetization distribution of the spin chain. We have entities that have the appearance of one-soliton-like shape, two-soliton-like shape, ... multisoliton-like shape with breathing motion.

Finally, due to the discrete nature of the lattice, the difference in the shape of the waves generated by MI processes strongly depends on the range of the values of the wavenumber of the carrier wave. They can be either extended or localized.

6. Energy distribution

The previous sections had addressed the study of a linear wave with small noise when an unstable region may exist. From the results of these previous sections it is clear that the energy initially concentrated in one mode will finally flow to all available modes in Fourier space.

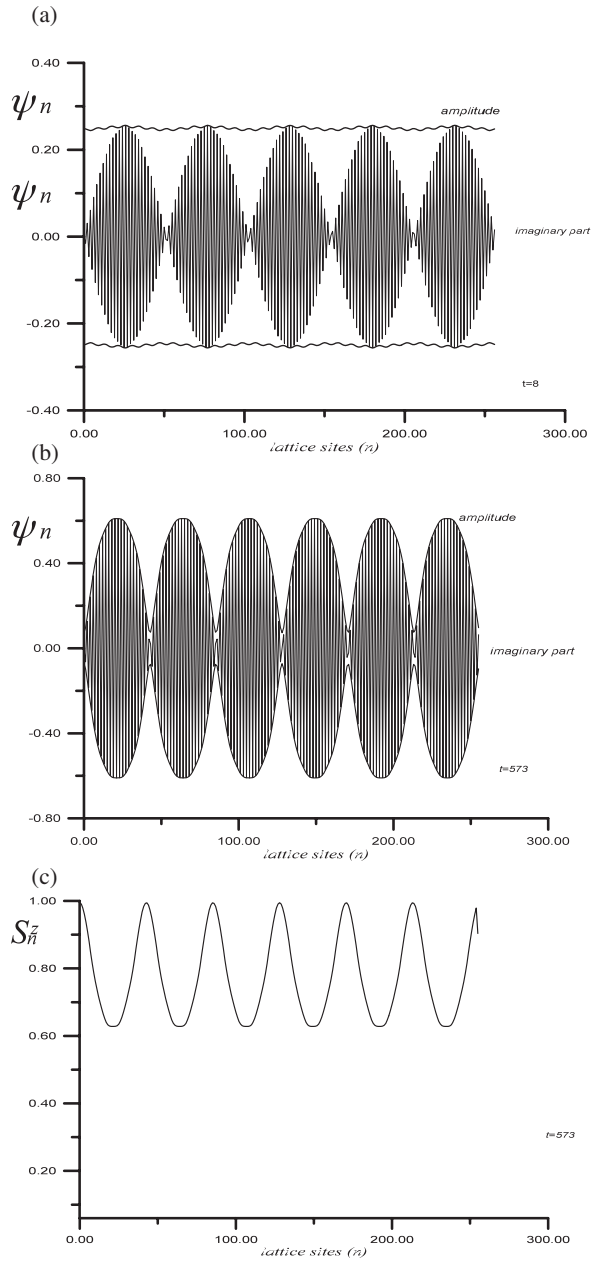

Figure 11. We show here only the imaginary part of the wavefunction Im (ψ_n), which is intercalated between the amplitudes $|\psi_n|$ obtained at different time MI processes. (a) The scheme of the spin wave representing the initial step of the MI process. We can see that, due to its modulation in the initial condition, the amplitude slightly oscillates around a constant value while the imaginary part is already modulated in the form a chain of soliton-like objects. (b) As for (a), the case of $p = 125$ obtained at time $t = 573$. It is clear to see how after a certain time the amplitude modulates in terms of a periodon that recovers completely the imaginary part of the wavefunction Im(ψ_n). (c) The spatial magnetization distribution S_n^z displays a periodon shape, which is constituted with periodic nonlinear excitations. (d) The creation of the chain of intrinsic localized modes in the scheme of S_n^z, which represents the spatial magnetization distribution. (e) We obtain only one intrinsic localized mode on the spatial magnetization distribution in the chain, corresponding to the case of $p = 127$.

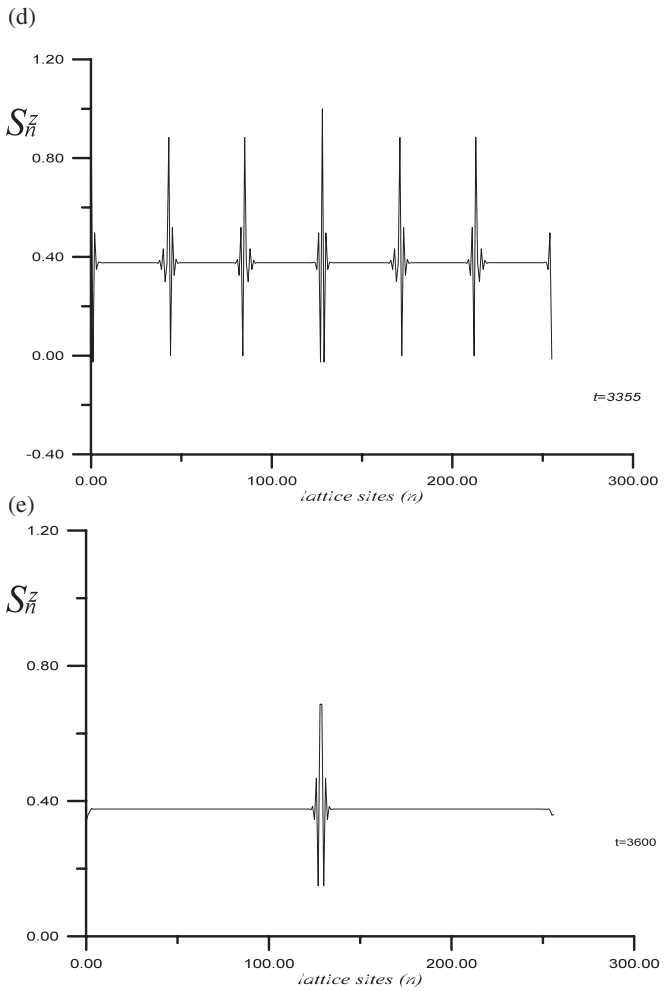

Figure 11. (Continued.)

For instance, due to the presence of additional harmonics in the spectrum, the energy is finally delocalized in Fourier space. It has also been demonstrated by Lai and Sievers [45] that a delocalized state in Fourier space can also be either a localized state or delocalized state in real space depending on the relative phase between the Fourier components. However, the Fourier space alone does not tell us the complete process of energy redistribution. However, it is generally believed that the physical system will finally reach equipartition of energy in a sufficiently long time since the entropy should grow during the system's time evolution. Otherwise, such a physical system should approach a state where the energy is evenly distributed not only among modes in Fourier space, but also on lattice sites in real space. A question that arises now is whether this excludes the possibility of energy localization at intermediate stages. Of course it does not, because one of the main effects of modulational instability is the creation of localized excitations from spatially extended excitations [46]. This modulational instability that induced energy localization has been proposed to be the mechanism responsible for the formation of intrinsic localization by many authors [46–48].

Precisely, it has been demonstrated in computer simulation that modulational instability can be used to generate intrinsic localized vibrational modes in nonlinear lattices via an optimal control scheme [48]. Indeed, the results of the previous section also confirm that with such a rigorous method intrinsic localized excitation can be generated in a ferromagnetic chain.

To investigate the creation of an intrinsic localized mode at an intermediate stage, we again use the same parameters as those corresponding to the result of figure 3 in a chain of 256 spins. At initial time (i.e. $t = 0$), the spins are coherently deviated with the initial condition of equation (4.3). To achieve our goal, we compute through a molecular dynamics simulation the time evolution of the energy density distribution defined in equation (4.1) for a few cases. Figures 12(a) and (b) depict the energy distribution on the spin chain at different intermediate stages, obtained with different initial conditions with wavevectors near the Brillouin zone boundary. From these figures, it is realized that the amplitude of an extended nonlinear spin wave grows smoothly for about 200 units of time (16 periods of the spin wave), while for longer times but still at an intermediate stage compared to the timescale of figure 3 the extended modes decay into slowly moving localized excitations. Thus, a number of localized excitations are created at the intermediate stage, but they should be trapped by discreteness effects for longer time. As deduced from the result of the previous section these localized excitations appear to last for a sufficiently long timescale. It would therefore be interesting for experimental purposes. Needless to mention, although localized excitations can be created in this way, it remains true that their lifetime depend on the biquadratic parameter and also the amplitude of the initial carrier wave. It is worth noting that the biquadratic exchange interaction influences not only the anharmonicity but also the discreteness of the lattice because, increasing the biquadratic parameter up to the range $0.5 < \alpha < 1$, and then also increasing the amplitude of the carrier wave, we realized that the lifetime of the localized excitations decreases. This is the proof that in such conditions the spin lattice is less discrete and less anharmonic. To obtain a more quantitative characterization, while taking into account the presence of an external applied magnetic field, we define the energy–energy correlation function as [49]

$$C_{\mathrm{E}}(n,t) = \left\langle \frac{\sum_{m}^{N-n} e(m,t)e(m+n,t) - \frac{1}{N-n}\sum_{m'}^{N-n} e(m',t)\sum_{m''}^{N-n} e(m'',t)}{\sum_{m}^{N-n} e^2(m,t) - \frac{1}{N-n}\sum_{m'}^{N-n} e(m',t)\sum_{m''}^{N-n} e(m'',t)} \right\rangle; \tag{6.1}$$

here, the symbol $\langle\cdots\rangle$ indicates an ensemble average over initial conditions and the function $e(m,t)$ is the energy density per site given in equation (4.1).

Since the initial condition corresponds to a linear wave, at the initial time, the system displays a uniform energy distribution as can be seen in figures 12(a) and (b). Thus $C_{\mathrm{E}}(n,0)$, is just a uniform background. While looking at figure 13, it is realized that, with increasing time for about 200 units of time, the instability destroys the linear wave and a maximum develops near $n = 0$. This maximum value of the energy–energy correlation function decreases as we move towards the spin chain. This behaviour is explained by localization of energy since it is not equally distributed on every spin lattice site. Furthermore, if we keep increasing the simulation time, it would happens that, in addition to the maximal value of the energy–energy correlation function near $n = 0$, which increases with time, a new maximum with greatest value occurs around the range $10 < n \leqslant 50$. This picture can be understood as a phenomenon of an increase of the number of localized modes with increasing time. The fact that this energy–energy correlation function confirms the localization phenomenon can be understood in the sense that, from our initial condition within such a Holstein–Primakoff approximation, there appear in the system magnon–magnon interactions. But since the magnon interaction in a ferromagnet with easy axis anisotropy is attractive in nature, they finally lead the initial spatially delocalized excitations to be characterized in the system by a tendency to accumulate in some region of space.

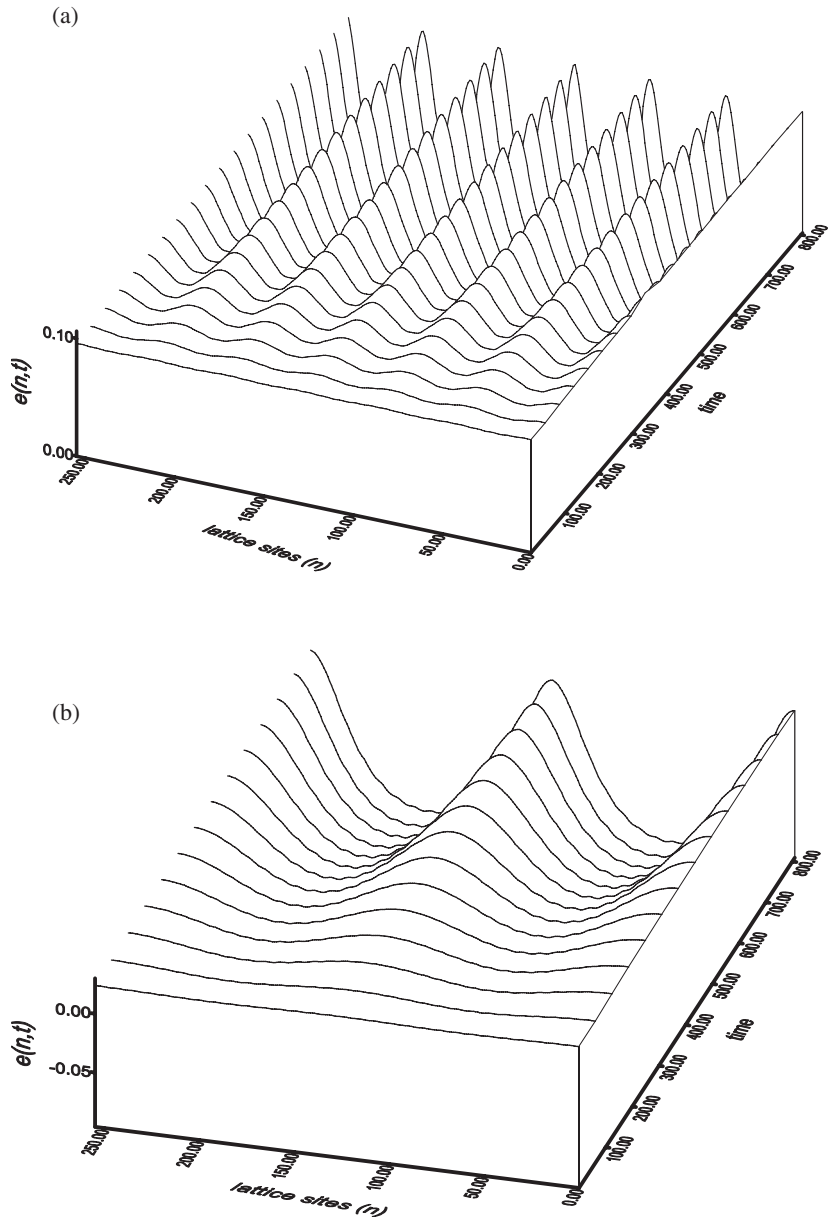

Figure 12. We show here the creation of intrinsic localized spin-wave excitations from an extended nonlinear spin wave via modulational instability. The biquadratic parameter is $\alpha = 0.06$. Plotted is the time evolution of the energy density distribution in real space. (a) $p = 125$; (b) $p = 127$.

7. Conclusion

We have investigated the modulational instability of extended nonlinear spin waves in a ferromagnetic chain with easy axis anisotropy. Our analysis revealed that some of the interesting features of the dynamics of a ferromagnetic spin chain, whose spins can deviate from the direction of the applied magnetic field, can be modelled with a discrete nonlinear

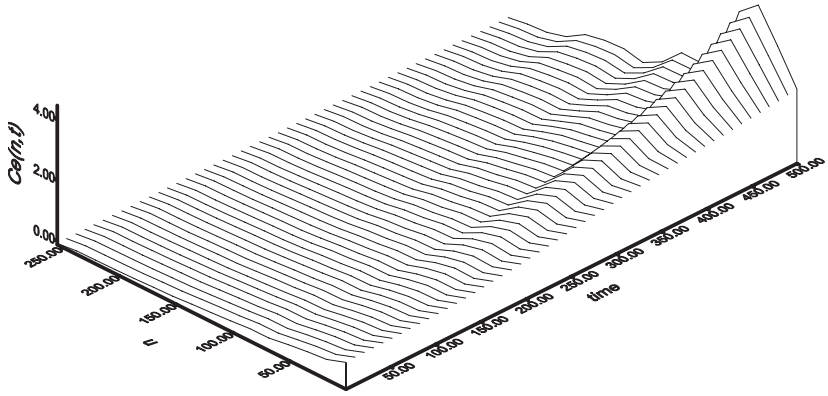

Figure 13. Energy–energy correlation function as a function of space and time. The curve is obtained here after averaging over ten initial conditions with the same parameters as those of figure 3.

Schrödinger-like equation (DNSL). This equation includes the effects of both linear and nonlinear terms. With an MI approach, we have shown that, depending on the strength of the biquadratic exchange energy relative to the normal exchange energy and then to the anisotropy energy, the stability domain in the (q, Q) plane can grow or reduce. When it reduces, more often, nonlinear spin waves both with short wavelength and long wavelength are stable to modulation for a large range of wavevector. We have illustrated here that, with periodic boundary conditions applied, a finite ferromagnetic chain of appropriate spin possesses a rich spectrum of both extended and intrinsic localized nonlinear spin excitations. One of the main features found for this discrete model for localized modes is the possibility of finding a long-lived intrinsic localized spin wave with wavevectors near the Brillouin zone boundary when the strength of the biquadratic exchange interaction relative to the normal exchange interaction is less than a certain limit i.e. $0 < \alpha \leqslant 0.5$, in which it becomes comparable to the anisotropy energy strength. This stability is also explained by the antagonist effects between the anisotropy interaction and the biquadratic exchange interaction. Therefore, our numerical simulations have demonstrated that, with a suitable choice of the biquadratic parameter, it is possible to create long-lived localized excitations by driving the ferromagnetic chain into a nonlinear regime. The presence of this localized excitation confirms the fact that in an easy-axis ferromagnet the magnons attract each other and this attraction is responsible for the phenomena that are associated with the appearance of spatially localized magnetic excitations.

Finally, the results demonstrate the importance and the potential of a simple, intuitive and physically appealing picture, which, even if it might not be quantitatively correct, reasonably describes the complex dynamics and certainly stimulates further experiments on magnetic model systems. The fundamental question for the existence of the new nonlinear excitations with soliton-like shape in a 1D ferromagnet, as suggested by our investigating theory, appears to have been answered positively by our numerical experiments. Needless to mention, for small- and medium-amplitude waves, the Holstein–Primakoff has precisely been introduced to be better than a classical limit. Nevertheless, this Holstein–Primakoff remains an approximation, and in the long term the role of the term that is neglected may become significant, i.e. the case of large nonlinearity. We want to stress that with about 180 periods of the spin wave, the early stage of modulational instability is probably better described by our Holstein–Primakoff approximation, but in our opinion it is obvious that 180 periods of a spin wave is a time which is still rather short with respect to the typical timescales of the spin-wave system to ensure the

validity of our study. It is however clear that, in order to determine the behaviour of the system on longer timescales, it would be necessary to go beyond the simple Holstein–Primakoff approximation. Therefore further computational, experimental and theoretical efforts in a next paper should now aim at the investigation of detail of these soliton-like objects bearing in systems where higher nonlinearity is taken into account at longer timescales, because higher orders in the amplitude would certainly enter when time becomes sufficiently large.

Acknowledgments

Dr Nguenang Jean-Pierre would like to thank the Agence Universitaire de la Francophonie (AUF) for providing him with a post-doctoral research grant at the Laboratoire de Physique de l'Ecole Normale Supérieure de Lyon, where this work was done. He would also like to acknowledge the warm hospitality of Professor Michel Peyrard at the Ecole Normale Supérieure de Lyon.

Appendix

We shall start this session by defining the coefficients of equation (2.8*b*),

$$A_1 = g_h - 2g_a; \qquad A_2 = -2g_\alpha - 1; \qquad A_3 = (g_{a-}g_\alpha)\varepsilon^2; \tag{A.1}$$

$$A_4 = \frac{(9g_\alpha - 1)\varepsilon^2}{4}; \qquad A_5 = \frac{(1 - 17g_\alpha)\varepsilon^2}{4}; \qquad A_6 = g_\alpha\varepsilon^2; \tag{A.2}$$

with

$$g_h = \frac{g\mu_B B}{J}; \qquad g_a = \frac{A}{J}; \qquad g_\alpha = \alpha(S_c)^2; \qquad S_c = \hbar S; \tag{A.3}$$

In order to define the difference of the matrix in equation (2.13), let us start by defining

$$\alpha_{01} = 2A_2\phi_0(\cos(Q) - 1)\cos(q) + A_3\phi_0^3 + 6A_4\phi_0^3\cos(Q)\cos(q) + 2A_5\phi_0^3\cos(Q) - 2A_6\phi_0^3(2\cos(Q) - 1)\cos(2q) \tag{A.4}$$

$$a_1 = -\alpha_{01}\phi_0, \qquad a2 = 0, \tag{A.5}$$

$$\alpha_{03} = -A_3\phi_0^3 - 2A_4\phi_0^3(2\cos(Q) - 1)\cos(q) - 2A_5\phi_0^3\cos(Q) + 2A_6\phi_0^3\cos(2q) \tag{A.6}$$

$$a_3 = -\alpha_{03}\phi_0 \qquad a4 = 0, \qquad c1 = 0, \tag{A.7}$$

$$c_2 = -2A_2(\cos(Q) - 1)\cos(q) - A_3\phi_0^2 + 2A_4\phi_0^2(3\cos(Q) - 1)\cos(q) - 2A_5\phi_0^2\cos(Q) + 2A_6\phi_0^2(2\cos(Q) + 1)\cos(2q) \tag{A.8}$$

$$c3 = 0, \qquad c_4 = -A_3\phi_0^2 - 4A_4\phi_0^4\cos(Q)\cos(q) - 2A_5\phi_0^2\cos(Q) + 2A_6\phi_0^2\cos(2q)$$

$$d1 = a3, \quad d2 = 0, \quad d3 = a1, \quad d4 = 0, \quad e1 = 0, \quad e2 = c4, \quad e3 = 0, \quad e4 = c2. \tag{A.9}$$

The polynomial coefficients of equation (3.6) are given by

$$\ell_0 = (c_2a_1)^2 + (a_3c_4)^2 - (a_1c_4)^2 \qquad \ell_2 = 2(c_2a_1 + a_3c_4); \tag{A.10}$$

from these coefficients, we can express

$$\alpha_1 = \frac{-l_2 - \sqrt{l_2^2 - 4l_0}}{2\phi_0^2}; \qquad \alpha_2 = \frac{-l_2 + \sqrt{l_2^2 - 4l_0}}{2\phi_0^2} \tag{A.11}$$

and finally

$$\Omega_{\mathrm{im1}} = \pm\sqrt{\frac{-l_2 - \sqrt{l_2^2 - 4l_0}}{2\phi_0^2}}; \qquad \Omega_{\mathrm{im2}} = \pm\sqrt{\frac{-l_2 + \sqrt{l_2^2 - 4l_0}}{2\phi_0^2}}. \tag{A.12}$$

The energy coefficients of equation (4.1) are defined by

$$e_1 = \left(g\mu_B B_e - 2A + \frac{J(1+2\alpha)}{2}\right)\varepsilon^2; \qquad e_2 = e_3 = \left(\frac{J(1+2\alpha)}{2}\right)\varepsilon^2;$$

$$e_4 = \left(A - \frac{J\alpha}{2}\right)\varepsilon^4; \tag{A.13}$$

$$e_5 = e_8 = -\frac{J\alpha}{2}\varepsilon^4, \qquad e_6 = \left(\frac{J(10\alpha-1)}{2}\right)\varepsilon^4; \qquad e_7 = \left(\frac{J(1-6\alpha)}{2}\right)\varepsilon^4; \tag{A.14}$$

It is important to notice that, to evaluate this energy term, there is a need to achieve some summations.

References

[1] Kjems J K and Steiner M 1978 *Phys. Rev. Lett.* **41** 1137
[2] Reiter G 1981 *Phys. Rev. Lett.* **46** 202
[3] Steiner M, Kakurai K and Knop W 1982 *Solid State Commun.* **41** 329
[4] Boucher J P, Regnault L P, Rossat-Mignot J, Renard J P, Bouillot J and Stirling W G 1980 *Solid State Commun.* **33** 171
[5] Tjon J and Wright J 1977 *Phys. Rev.* B **15** 3407
[6] Haldane F D M 1983 *Phys. Rev. Lett.* **50** 1153
[7] Mikeska H J and Steiner M 1991 *Adv. Phys.* **40** 191
[8] Nguenang J P and Kofané T C 1997 *Phys. Scr.* **55** 367
[9] Nguenang J P, Kofané T C, Yomba E and Yo J D 1999 *Phys. Scr.* **60** 460
[10] Nguenang J P, Kenfack A J and Kofané T C 2002 *Phys. Rev.* E **66** 56613
[11] Nguenang J P and Kofané T C 2000 *Physica* D **147** 311
[12] Radcliffe J M 1971 *J. Phys. A: Math. Gen.* **4** 313
[13] Balakrisnan R and Bishop A R 1985 *Phys. Rev. Lett.* **55** 537
[14] Holstein T and Primakoff H 1940 *Phys. Rev.* **58** 1098
[15] Glauber R J 1963 *Phys. Rev.* **131** 2766
[16] Sievers A J and Page J B 1995 *Dynamical Properties of Solids* vol 7, ed G K Horton and A A Maradudin (Amsterdam: North-Holland) p 137
[17] Flach S and Willis C R 1998 *Phys. Rep.* **295** 181
[18] Dolgov A S 1986 *Sov. Phys.—Solid State* **28** 907
[19] Sievers A J and Takeno S 1988 *Phys. Rev. Lett.* **61** 970
[20] Burlakov V M, Kiselev S A and Pyrkov V N 1990 *Phys. Rev.* B **42** 4921
[21] Page J B 1991 *Phys. Rev.* B **41** 7835
[22] Sandusky K W, Page J B and Scmidt K E 1992 *Phys. Rev.* B **46** 6161
[23] Dauxois T and Peyrard M 1993 *Phys. Rev. Lett.* **70** 3935
[24] Cai D, Bishop A R and Gronbech-Jensen N 1994 *Phys. Rev. Lett.* **72** 591
[25] Kiselev S A, Bickhann S R and Sievers A J 1994 *Phys. Rev.* B **50** 9135
[26] Takeno S and Kawasaki K 1992 *Phys. Rev.* B **45** R5083
[27] Takeno S and Kawasaki K 1994 *J. Phys. Soc. Japan* **63** 1928
[28] Wallis R F, Mills D L and Bordmann A D 1995 *Phys. Rev.* B **52** R3828
[29] Rakhamanova S and Mills D L 1996 *Phys. Rev.* B **54** 9225
[30] Lai R, Kiselev S A and Sievers A J 1997 *Phys. Rev.* B **56** 5345
[31] OhiShi J, Kubota M, Kawasaki K and Takeno S 1997 *Phys. Rev.* B **55** 8812
[32] Lai R and Sievers A J 1998 *Phys. Rev. Lett.* **81** 1937
[33] Lai R and Sievers A J 1999 *Phys. Rep.* **314** 147
[34] Ferrer R 1985 *Physica* B&C **132** 56
[35] Adler J 1979 *PhD Thesis* University of New South Wales
[36] Anderson P W 1959 *Phys. Rev.* **15** 2
[37] Kapor D V and Skrinjar M J 1987 *Europhys. Lett.* **3** 953
[38] Zhang W M, Feng D H and Gilmore R 1991 *Rev. Mod. Phys.* **62** 867
[39] Benjamin T B and Feir J E 1967 *J. Fluid. Mech.* **27** 417
[40] Bespalov V I and Talanov V I 1966 *Pis. Zh. Eksp. Teor. Fiz.* **3** 471

[41] Tanuiti T and Washimi H 1992 *Phys. Rev. Lett.* **21** 209
[42] Cottam M G 1994 *Linear and Non Linear Spin Waves in Magnetic Films and Super Lattices* (Singapore: World Scientific)
[43] Kiselev S A, Bickhann S R and Sievers A J 1995 *Comments Condens. Matter Phys.* **17** 135
[44] Swarz U T, English L Q and Sievers A J 1999 *Phys. Rev. Lett.* **83** 223
[45] Lai R and Siever A J 1998 *Phys. Rev.* B **57** 3433
[46] Tai K, Tomita A, Jewell J L and Hasegawa A 1986 *Appl. Phys. Lett.* **49** 236
[47] Daumont I, Dauxois T and Peyrard M 1997 *Nonlinearity* **10** 617
[48] Rossler T and Pages J B 1997 *Phys. Rev. Lett.* **78** 1287
[49] Landau D P and Binder K 2000 *A Guide to Monte Carlo Simulations in Statistical Physics* (Cambridge: Cambridge University Press) p 100